

MAR 10 1947

477

NATIONAL ADVISORY COMMITTEE FOR AERONAUTICS

TECHNICAL NOTE

No. 1128

AN INVESTIGATION OF THE AERODYNAMIC CHARACTERISTICS OF A ROTATING AXIAL-FLOW BLADE GRID

By John R. Weske
Case School of Applied Science



Washington
February 1947



3 1176 01425 7910

NATIONAL ADVISORY COMMITTEE FOR AERONAUTICS

TECHNICAL NOTE NO. 1128

AN INVESTIGATION OF THE AERODYNAMIC CHARACTERISTICS
OF A ROTATING AXIAL-FLOW BLADE GRID

By John R. Weske

SUMMARY

The report contains the results of an experimental investigation of the aerodynamic characteristics of a rotating axial-flow blade grid with pressure-increasing effect. Several techniques of measurement were applied: namely, pressure distribution measurements, pitot tube, and hot wire wake surveys. The results of these measurements were used as the basis of an analysis of the flow through the rotating grid, in particular, of those effects not present in a fixed grid and of the factors not accounted for in the two-dimensional theory of axial-flow blade grids.

It was found that radial displacement of the boundary layer delays the stall of the root section and induces early stall of the tip section which may become critical for the pumping limit of the blade row. Interaction of boundary layers along the casing and the hub and along the blade surfaces through radial flow represents a major factor not accounted for in the two-dimensional theory of blade grids. Of similar importance upon efficiency and operating characteristics is the radial displacement of the wakes.

INTRODUCTION

When using the results of flow tests of model grids as a basis for the performance calculation of rotating axial-flow blade rows, questions arise in regard to the applicability. Model grids often are straight rather than annular, in most cases they have a finite number of blades, and the variation of conditions of flow along the span in no wise corresponds to that of the annular grid. Most important of all, certain effects of centrifugal acceleration present in the rotating grid cannot be simulated in a static-flow test. In order to find an answer to these questions, fundamental investigation of the

flow through a rotating blade grid appeared desirable. Investigations on rotating blade grids have the advantage over static flow tests that higher Reynolds and Mach numbers can be attained without requiring a large amount of power for moving the air; furthermore the requirement of an infinite number of blades is automatically realized. Experimental techniques, which should correspond to those customary in static-flow tests, however, are considerably more cumbersome.

The attempt was made to develop suitable experimental methods and with their aid to measure and analyze the characteristics of a rotating axial-flow grid, for which a suitable profile and specified operating conditions had been proposed by the National Advisory Committee for Aeronautics, particularly in those respects in which they differed from those of the fixed grid. A retarding grid was chosen partly because it requires a less complicated test setup than an accelerating grid, but primarily because the particular effects distinguishing the action of the rotating and the stationary grid were anticipated to stand out more distinctly.

This investigation, conducted at the Case School of Applied Science, was sponsored by and conducted with the financial assistance of the National Advisory Committee for Aeronautics.

The tests were conducted by Mr. R. J. Carleton, research assistant, and Mr. Robert Christiansen, a student of that institution. The calculations were carried out by Mrs. F. Scott Rodgers, research assistant.

LIST OF SYMBOLS AND COEFFICIENTS

r radius, feet

y distance parallel to the axis of the blade grid, that is, in peripheral direction, feet

b number of blades

$t = \frac{2\pi r}{b}$, pitch of blades*, feet

l chord of blade element*, feet

ω angular velocity of the blade grid, radians per seconds

$u = rw$ rotational velocity of the blade at radius r , feet per second

*(Note: Quantities marked by an asterisk are shown on fig. 11.)

- c absolute velocity*, feet per second
- w velocity relative to the blade element*, feet per second
- β angle of the relative velocity with respect to the grid axis (see subscripts) or: angle of the reference chord of the blade with respect to the grid axis*
- R resultant force per unit spanwise length on the profile*, pounds
- N component of R normal to the chord*, pounds
- C component of R parallel to the chord*, pounds
- $$\delta = \cos^{-1} \left(\frac{N}{R} \right) = \tan^{-1} \left(\frac{C}{N} \right)^*$$
- S = R cos ($\beta + \delta$) component of R normal to the grid*, pounds
- T = R sin ($\beta + \delta$) component of R parallel to the grid*, pounds
- L lift force per unit span*, pounds
- D drag force per unit span*, pounds
- ϵ angle between L and R*, degrees
- $\alpha = \beta - \bar{\beta}$ angle of attack*, degrees
- $$a = \frac{DC_L}{D\alpha}$$
- slope of the lift curve
- $a_\infty = 2\pi/57.3$ slope of the theoretical lift curve of a thin airfoil of zero camber
- p static pressure, pounds per foot
- q velocity pressure, pounds per foot
- Γ circulation, feet per second
- A aspect ratio
- Subscripts
- 0 refers to free stream just outside the wake

*(Note: Quantities marked by an asterisk are shown on fig. 11.)

- 1 refers to the plane at inlet of the grid
- 2 refers to the plane at outlet of the grid
- u denotes component in circumferential direction
- m denotes component in axial direction

Superscript

- refers to mean condition in the grid, for example

$$\bar{w} = \sqrt{w_{1\bar{u}}^2 + \left(\frac{w_{1\bar{u}} + w_{2\bar{u}}}{2}\right)^2} *$$

$$\bar{q} = \rho \frac{\bar{w}^2}{2}$$

Coefficients

$$C_L = \frac{L}{l\bar{q}} = \frac{R \cos (\beta + \delta - \bar{\beta})}{l\bar{q}} \quad \text{lift coefficient of the blade section}$$

$$C_D = \frac{D}{l\bar{q}} = \frac{R \sin (\beta + \delta - \bar{\beta})}{l\bar{q}} \quad \text{drag coefficient of the blade section}$$

DESCRIPTION OF APPARATUS

The Test Stand

The test stand for the rotating blade grid shown in figures 1 and 2 was essentially a cylindrical air duct of 36 inches diameter, the central section of which housed the grid and its driving motor, a 7½ horsepower, 1750 rpm, direct-current motor with Ward-Leonard control. The motor was cowled by a cylindrical casing of the same diameter as the hub of the grid. Stationary fairing pieces upstream of the grid and downstream of the motor cowling lessened interferences of the flow and established rotational symmetry which is disturbed upstream only.

* (Note: Quantities marked by an asterisk are shown on fig. 11.)

by slender radial brackets supporting the nose section and downstream of the grid by the cylindrical motor columns of 1-5/6-inch diameter and the corners of the motor base. The length of the ducting between the inlet bellmouth and the center section was chosen with a view to obtaining accurate measurements of the quantity of flow at the throat of the bell-mouth, that of the outlet ducting, to avoid flow interference from the throttle cone or the booster fan, either of which could be placed at the outlet.

The Blade Grid

The rotating blade grid (fig. 3) has the following dimensions: 20 inches hub diameter, 36 inches tip diameter, 8 inches axial width. It consists of 12 equally spaced blades of identical shape and of equal angular setting, mounted between the hub and a shroud ring. A rotating shroud ring was chosen to obtain a wheel of sufficient strength and rigidity. While radial clearances thereby were eliminated, the design made necessary annular axial clearances of approximately one-eighth inch width on either side of the shroud ring.

The blades were made of cast methyl methacrylate resin, which was found highly suitable. They were machined as a cylinder to template of 7-inch chord of an airfoil furnished by the National Advisory Committee for Aeronautics (fig. 4) polished to a smooth aerodynamic surface, then heated to 255° F and given the required twist in a plaster case die mold. The mold insured uniform shape of all blades. This process admitted of modification of the twist of the blades, if necessary.

In order to establish the pitch and twist of the blades a first attempt was made to design the grid for a blade angle, solidity and lift coefficient on mean radius for which a chordwise distribution of pressure difference had been determined theoretically by the National Advisory Committee for Aeronautics. With the assumption of constancy of circulation along the radius, this condition, which will be referred to as the "specified" condition, however, led to an excessively large blade angle and lift coefficient at the root. For this reason a different condition was selected as the "design" operating condition, at which the lift coefficient of the mean station was chosen $C_L = 1.0$ compared to $C_L = 1.26$ for the specified condition. Blade angle and solidity on mean radius correspond to the specified values, and the axial velocity and circulation were made constant along the radius at this design condition. The following factors were considered in the calculation:

- (a) The zero lift angle of attack in grid arrangement was determined for the thin circular-arc airfoil corresponding to the given blade profile (reference 1, p. 65).

- (b) Correction was made for grid interference due to circulation (reference 1, p. 40).
- (c) Further correction was made for grid interference due to thickness of the blades (reference 2).
- (d) No account was taken of the drag, as its magnitude was unknown.

The results are given in the tabulation below:

GRID DATA AND BLADE ANGLES

Section	Radius (in.)	Chord, l (in.)	Pitch, t (in.)	Blade angle
Tip section	18	7	9.43	35° 00'
Outer section	17	7	8.90	37° 23'
Middle section	14	7	7.34	47° 30'
Inner section	11	7	5.77	57° 37'
Root section	10	7	5.25	60° 00'

One of the 12 blades, to be referred to as the master blade, (fig. 5), is provided with numerous pressure taps of 0.02-inch diameter arranged in three cylindrical stations, one "outer" ($r = 17$ in.), one "middle" ($r = 14$ in.), and one "inner" ($r = 11$ in.) station, 23 taps to each station, distributed over both sides of the blade, as shown in figure 4. Care was taken in the drilling, first to locate all taps of a given section on the same radius, in order to eliminate error in pressure measurement, and second, to place corresponding taps of the three sections at the same chordwise position.

The Selector Switch and Seal

Pressures on the surface of the blade section were transmitted to the stationary system through a selector switch and a seal, shown in figure 6. The rotating element of this switch had 24 connections, 22 of which lead to pressure connections on the master blade. The remaining 2 taps were used as "blind taps" to indicate the position of the

selector switch while the unit was in operation. By a latch device, operated from outside the test section by axial shift motion, it was possible to connect each pressure line successively to the central pressure bore. From here, the pressure was transmitted to the stationary system through a seal. The contact surfaces for the pressure duct at the selector switch and at the seal were made of soft rubber. A lubricating system supplied glycerine to the seal to help maintain the airtight contact of the sliding surfaces.

The Pitot-Tube Traversing Device

The equipment developed for obtaining traverses across the wake of the blade in the rotating system is shown in figure 7. The pitot tube used for this purpose was of special design insofar as it had a removable screwed-in tip containing the static pressure holes. With the tip in place the pitot tube would read the static pressure; while by removal of the tip it could be changed to a total pressure tube. The proportions of the pitot tube corresponded to those of a Prandtl tube; its diameter was 0.08 inch.

The pitot tube could be placed at any spanwise position of the blade in a plane tangent to the concentric cylinder by adjustment of the holder, and moved circumferentially from without the test section by a pulley-and-lever mechanism while the grid was rotating. A sighting window in the casing permitted stroboscopic observation of the position of the pitot tube.

The Hot-Wire Equipment

The arrangement of the apparatus used for obtaining oscillographic records of axial velocity profiles downstream of the rotating grid is shown schematically in figure 8.

The hot-wire instrument used for this work has been described elsewhere (reference 3) for which reason a description is omitted here, except for the mention of two of its characteristics, namely, the linearity of its reading with velocity and its rapid response to fluctuations, by virtue of which the instrument gives readings of the arithmetic mean velocity of a fluctuating stream, and secondly, its directional characteristics by virtue of which it is possible to read the mean as well as the instantaneous velocity component normal to the hot wire.

The hot-wire filaments were inserted through small openings provided in the casing immediately downstream of the rotating grid. To coordinate the recording of the oscillograph pattern of the velocity fluctuation with the passing of a particular blade, there was developed a trigger circuit and external sweep generator operated by a light beam

reflected upon a photoelectric cell from a small mirror rotating with the blade grid. The sweep produced by the circuit had a constant speed, making the distance along the abscissa on the oscillograph proportional to distance in circumferential direction of the rotating grid. Selection of the blade interval to be investigated was made by placing the light and photocell unit in the proper peripheral position.

TEST PROCEDURE

Basic Measurements and Calibration Tests

The quantity of flow was determined from a static pressure reading at the center of the throat of the bellmouth, which had been calibrated against pitot-tube traverses.

Profiles of axial velocities versus radius immediately (8 in.) upstream and 10 inches downstream of the grid at various ratios: mean axial velocity through the grid to tip speed, $\frac{w_m}{u} 8/y$ representing calibration data are shown in figure 9 as they are of interest for the evaluation of test results.

The presence of the columns supporting the motor in the air stream downstream of the grid was found to affect the flow at the outlet of the grid only very slightly, and it was concluded that this interference might be neglected.

The investigation of the leakage across the axial clearances of the rim disclosed that the thrust acting on the wheel decreased the forward clearance to less than one-eighth inch. No inward flow was noticeable through the clearance since windage counteracted this flow. Windage also made impossible an exact determination of the outward flow through the downstream clearance. This flow varied greatly with the back-pressure on the wheel. At maximum lift coefficient of the blades it did not exceed 2 feet per second or approximately five percent of the quantity of flow.

Measurements of Pressure Distribution

The accuracy of pressure distribution measurements on the rotating blades was checked by repeating the first few readings at the end of each series of measurements, there being no independent method of calibration. Comparison of the pressure measurement nearest to the stagnation point of the blade with a total pressure measurement from a fixed pitot tube placed immediately ahead of the grid served as another check. It was not necessary to determine the effect of centrifugal force upon the air in the rotating pressure leads separately since the results

are based upon pressure differences rather than upon the absolute value of pressures. The principal series of tests consisted of measurements of the pressure distribution over the three selected blade stations $r = 11$ inches, $r = 14$ inches, and $r = 17$ inches. Conditions of operation were varied either by change of speed of the booster fan or by adjustment of the throttling device. The speed of rotation of the grid was 900 to 1000 rpm except for tests requiring a booster fan, in which it ranged from 350 to 880 rpm. This reduction was necessary to remain within the limits of capacity of the booster fan. The tests covered a range of Reynolds numbers based upon the chord of the blade and the mean relative velocity past the blade of $R = 300,000$ to $R = 620,000$ for the middle section.

Pitot-Tube Wake Traverses

Alinement of the pitot tube with respect to the flow was obtained by stroboscopic observation of a silk thread attached to the head of the pitot tube. The variation of direction as indicated by the thread was less than $\pm 10^\circ$ relative to the pitot tube, which was considered to be within allowable limits. What was said in regard to pressure measurements in the preceding paragraph also applies to pitot tube measurements, particularly that it was not necessary to account for the effect of centrifugal force in the rotating leads explicitly.

The wake traverses relative to the rotating blade grid were taken behind the master airfoil at the same operating conditions as the pressure distribution measurements; the surveys extended over the Reynolds number range from $R = 300,000$ to $R = 620,000$ for the middle section. The axial distance of the tip of the pitot tube from the trailing edge of the blade varied from $1/4$ to 1.6 inch and is stated in conjunction with the test results. In general, the operating conditions were adjusted to operate at the lift coefficient of the corresponding pressure distribution measurements. This was done to establish correspondence of the drag coefficients calculated from measurements obtained by the two techniques.

Static pressure measurements were taken immediately after the run for total pressure measurements, a brief stop being necessary to insert the tip which converted the total pressure tube into the static pressure tube.

Hot-Wire Measurements

Hot-wire measurements were obtained for a selected number of operating conditions corresponding to those of the pressure and pitot-tube traverse measurements. The hot wire was oriented in the plane of

rotation approximately one inch downstream of the trailing edge and tangential to a concentric circle. The mean velocity reading of the hot wire instrument was continuously checked against the axial velocity calculated from a corresponding directional pitot tube reading. The operating conditions for the hot-wire traverse measurements correspond to those of the pitot-tube traverses.

Direction of Flow in the Boundary Layer of the Blades

Measurements of the direction of flow along the surface of the blades were undertaken for the purpose of explaining certain discrepancies between the drag as determined from pressure distribution and wake traverse measurements. While no simple method was discovered for the measurements of the radial component of velocity in free stream of the rotating grid since silk threads are deflected by centrifugal force and smoke vane difficult to observe in stroboscopic light, a method described by Ruden (reference 2) utilizing the chemical discoloring action of ammonia vapor upon Ozalid paper proved applicable in the boundary layer.

Ozalid paper was glued smoothly to the blade surface, and ammonia vapor was introduced through the pressure ducts and emitted from pin holes in the paper. A set of traces was produced by the ammonia-vapor method at selected points on both sides of the airfoil.

RESULTS AND DISCUSSION

Lift and Pressure Drag of the Blade Sections

Figure 10, a to c, show a number of pressure distributions in non-dimensional form plotted versus distance along the chord for the middle, outer, and inner blade stations, respectively.

From the pressure distributions (fig. 10, a to c) were calculated successively the normal force component per unit of spanwise length, N and the chordwise force component C , the resultant force R and its direction with respect to the plane of the rotation of the grid, finally, the lift coefficient C_L and the "pressure" drag coefficient C_D . The geometrical relation of these quantities may be seen from the velocity diagram (fig. 11).

The specifying term "pressure" drag is used here because inherently the method of measurement yields only a portion of the drag, namely, the part due to the deviation of the pressure distribution from that corresponding to potential flow. No account is taken of the direct effect of skin friction. It has been shown that in grids of high

solidity the pressure drag does not differ greatly from the profile drag of the airfoil (reference 4).

Aerodynamic Characteristics of the Blade Sections

Curves of the lift coefficient C_L versus angle of attack α and versus C_D are shown in figure 12. The $C_L - \alpha$ curves for all three stations of the blade show straight portions in the range of low positive angles of attack. As the C_L increases, both the outer station and the middle station are subjected to a gradual stall extending over a wide range of angles of attack. The maximum lift coefficient of the outer stations is smaller than that of the middle stations and its stalling region begins at a low value of C_L . The inner station, however, reveals no evidence of stall. In fact, at large lift coefficients the test points fall considerably above the straight line. This and a corresponding deviation at negative C_L may be explained by radial displacement of the flow (see fig. 9) at these conditions which differ greatly from the design condition.

According to figure 12 the zero lift angle of attack varies 6° from the inner to the outer station. Since the blade was not designed for this operating condition, radial displacement of the flow (see fig. 9) precludes close correlation by the two-dimensional theory. The following factors, however, may be considered.

I. Grid Interference Originating from Vortex Fields

Thin airfoil grid theory of cambered profiles (reference 1) leads to a variation of zero lift angle of attack of less than 1° between the three sections. Consequently, this is an effect of minor importance.

II. Thickness Interference

Variation of angle of attack caused by the thickness of the blade sections, calculated by the method of references 2 and 5, requires a correction of $-1^\circ 20'$ for the outer section and of $+2^\circ 37'$ for the inner section and is not negligible.

III. Relative Rotation

The air, having no rotation initially, rotates in each blade interval relative to the grid, in direction opposite to that of the grid

at an angular velocity equal to the angular velocity of the grid. Relative rotation produces: (a) peripheral velocities on the surface of concentric cylinders which are of interest in choosing the blade angles, and (b) velocities in radial direction.

The effect of relative rotation cannot be appraised readily since the impeding action of friction is not sufficiently known.

Thickness effect appears to be the major factor causing variation of zero lift angle of attack of the three blade sections. It is noted that the calculated thickness correction is of the same sign and magnitude as the variation of zero lift angle of attack measured.

At the angle of attack corresponding to the specified operating condition $\alpha = 29^\circ 29'$ for the middle section, figure 12 shows measured lift coefficients of $C_L = 0.88$ to 0.98 , marked by a circle. The theoretical expectation for this condition was $C_L = 1.26$. A partial explanation for this pronounced discrepancy may be derived from a calculation of the effective aspect ratio related to the slope of the measured lift curve by the equation

$$A_{\text{eff}} = \frac{1}{\pi \frac{a_{\infty} \alpha}{a} - a} \quad \text{where} \quad a_{\infty} = \frac{2\pi}{57.3}$$

The effective aspect ratios thus calculated are:

$$A_{\text{eff}} = 2.14 \quad \text{for the outer station}$$

$$A_{\text{eff}} = 6.00 \quad \text{for the middle station}$$

$$A_{\text{eff}} = 2.27 \quad \text{for the inner station}$$

The slope of the theoretical lift curve for infinite aspect ratio is drawn in figure 12 in dot and dash for comparison.

The lift coefficients at the specified condition of the middle station may now be calculated from the angle of attack with respect to the zero lift point, for infinite aspect ratio (slope $a_{\infty} = \frac{2\pi}{57.3}$) $C_L = 1.31$

and for aspect ratio $A_{\text{eff}} = 6.0$, $C_L = 0.99$, giving rather good agreement with the measured results.

A comparison of the measured pressure distribution of the middle station for the specified operating condition and of the corresponding theoretical pressure distribution was made in figure 13. The former

was calculated by the National Advisory Committee for Aeronautics for $C_L = 1.26$ and is constant from the leading edge to the 50-percent chord point, beyond which it decreases linearly to zero at the trailing edge. The latter is the pressure distribution curve marked $C_L = 0.88$ of figure 10a replotted to scale. In consideration of the effect of aspect ratio discussed above it may not be expected anything more than a general resemblance is established, and this resemblance obviously exists.

Profile Drag

Results of profile drag calculations from the pitot-tube wake traverse patterns taken at 880 rpm and shown in figure 14 are tabulated below:

Station	r (in.)	C_L	C_D from wake traverse
Outer	17	0.545	0.1315
Middle	14	.72	.0429
Inner	121/8		.0487
Inner	11	.516	.1456

The patterns at $r = 11$ inches and at $r = 17$ inches clearly are affected by the boundary layer at the hub and the casing, respectively.

Drag coefficients for these and other measurements were obtained by evaluation of the equation

$$C_D = \frac{2}{l} \left[\int_{\text{wake}} \left(\frac{w}{w_0} \right) dy - \int_{\text{wake}} \left(\frac{w}{w_0} \right)^2 dy \right]$$

A typical oscillograph of a hot-wire wake traverse of axial velocity components is shown in figure 15 for the middle station at $C_L = 0.72$ and $R = 500,000$. In calculating the profile drag from these records, no account was taken of the deviation of the direction of flow from the mean direction, a simplification generally made in the evaluation of wake profiles for determination of profile drag. For $\beta = \text{constant}$ the above equation for C_D may be rewritten in terms of the axial component of velocity

$$C_m = w/\cos \beta \quad \text{and} \quad C_{mo} = w_o/\cos \beta$$

It is seen that the angle β may be eliminated and the equation reads

$$C_D = \frac{2}{\pi} \left[\int_{\text{wake}} \left(\frac{C_m}{C_{mo}} \right) dy - \int \left(\frac{C_m}{C_{mo}} \right)^2 dy \right]$$

The drag coefficients calculated from pitot-tube and hot-wire traverses have been correlated with pressure drag coefficients versus the corresponding lift coefficients for the inner, middle, and outer station in figures 16a, 16b, and 16c, respectively. A few drag coefficients taken at other specially designated radii were also shown in these graphs.

Further test results relating to the question of drag of rotating blades are given in figure 17, which is a particular sample taken at $C_L = 0.72$ and $R = 500,000$ for the middle section of vapor trace records at various points on both sides of the surface of the blade. Finally, a comparison is made of wake traverse profiles of axial velocities obtained by the pitot-tube and the hot-wire methods at identical operating conditions:

$$C_L = 0.72, \quad R = 500,000, \quad \text{for the middle section (Fig. 18).}$$

The following conclusions may be drawn from figures 16a to 16c, 17, and 18.

(a) The drag coefficients obtained by the three different methods agree between $C_L = 0.5$ and 0.7 at the middle station. The minimum value $C_D = 0.03$ at this and the inner station is only slightly larger than might be anticipated in view of the large thickness ratio of the profiles.

(b) Maximum L/D ratio occurs at lift coefficients much lower than design lift coefficients, which suggests that a profile of larger camber, for which presumably the (L/D) maximum occurs at higher C_L , would be more suitable, particularly for the inner and middle stations.

(c) Drag coefficients from wake traverses of the inner and outer stations are considerably larger than the pressure drag coefficients. While the diffuser effect associated with the decay of the wake

downstream of the grid may be suggested as a cause of this discrepancy, it appears that the principal factor is the radial outward displacement of the wake and of the boundary layer of the hub (the latter flowing outward in the wind shade of the blade), as shown by wake traverse results at various radii larger than that of the inner station (specially marked on fig. 17a) and smaller than that of the outer section (specially marked on fig. 17c) which establish a gradual transition.

If radial displacement of the wake is taken into account, the widely divergent values of pressure and wake traverse drags may be reconciled. Conversely, it might be stated that drag measurements by the experimental methods applied are not conclusive unless the effect of radial displacement of flow is known.

(d) While radially outward motion in the boundary layer along the back of the blade is clearly indicated in figure 17, it is absent along the front of the blade, probably because of the rotation of the body of air relative to the grid. This renders the structure of the wake more complicated, not, however, to the extent of the invalidating the results of wake traverse measurements. Another factor of a qualitative nature are erratic fluctuations of the hot-wire wake profile of the tip station near the stalling condition of that section, presumably from interaction of the boundary layer of the casing and of profile wakes. These fluctuations, though not discernible in corresponding pitot traverses, tend to limit the reliability of the latter. In the absence of more accurate or quantitative information it is merely suggested that the observed instability precedes or may even be the cause of stalling at the tip which, in turn, may initiate pumping even before the root section has reached the stalling point.

(e) Although the agreement of pitot and hot-wire traverses shown in figure 18 may not be as close as may seem desirable, the comparison serves to emphasize that the hot-wire traverse method, which is much simpler than the other methods of drag measurement employed may be expected to give useful quantitative results.

(f) Summarizing the analysis of the profile drag of the rotating grid, it is evident that the boundary layers at the hub and at the casing have a large influence upon the drag characteristics of the blade. While it is regretted that measures toward decrease of these boundary layers (shortening of the approach lengths; redesign of the upstream portion of the hub) could not be taken, there is some justification to assume that the operation of rotating grids in multistage units takes place in the presence of "end effects" not unlike those of the test grid.

(h) The rational design of a grid in which each blade section is adapted closely for optimum performance at design condition would require advance knowledge of the drag as well as of the lift characteristics

of the various blade sections. Furthermore it would call for variation along the span, of the camber and thickness of the airfoil section in addition to blade angle variation.

Correlation of Grid Performance Calculated from Profile Characteristics
with Measured Performance

Variation of circulation with radius. - The circulation about the blade section was calculated from the equation

$$\Gamma = \frac{C_L l w}{2}$$

The quantity Γ/u was then formulated to correct for rotative speed and plotted against w_m/u in figure 19. The three curves of this graph for the three blade stations seem to indicate the following:

- (a) Constant circulation over the middle and outer stations is maintained over a very wide range of operating conditions including the design condition.
- (b) The circulation of the inner section is considerably less than the middle and outer sections for all but very light loads of the grid. This may be attributed in part to boundary layer effects which may be accentuated in view of the large drag of this section, and in part to neglect of rotation of the air relative to the grid in the choice of the blade angles.
- (c) The stalling points of the middle and outer sections are closely interrelated and maximum circulation occurs at nearly the same operating condition.
- (d) The inner section was not affected by the stalling of the middle and outer parts. The circulation continued to increase as the load on the grid was increased without indication of a stall. The highest Γ values that could be realized with the test apparatus closely approach the maximum of the outer and middle stations.
- (e) The curves suggest the possibility of designing blades for constant circulation along the radius, even though this will lead to very large lift coefficients at the root. This, however, would require prior verification by test, which was not undertaken in the present investigation.

Static Pressures

A nondimensional static pressure increase $\Delta p/q_u$ was calculated for a number of test points for each blade section as follows:

$$\Delta p/q_u = c_1 \frac{1}{t} \cos\bar{\beta} (1 - \tan \epsilon \tan\bar{\beta}) \left(\frac{w}{u} \right)^2$$

where

$$q_u = \rho \frac{u^2}{2}$$

and plotted versus w_m/u in figure 20.

Thus the three solid curves were obtained for the three sections. Corresponding curves (dotted lines) were plotted from the measured static pressure increase across the grid. In calculating the latter, the friction drop in the duct was taken into account and a linear variation of static pressure between the hub and tip was assumed instead of the unknown actual variation. As might be expected in view of the fact that the grid produces a vortex at discharge, the static pressure rise across the grid increases with the radius. This fact is brought out by the vertical displacement of both the measured and the calculated curves for the three sections with respect to each other.

In the region of the design operating condition the measured values for the inner and middle stations are but slightly below those calculated from the profile characteristics; those for the outer station differ by 5 percent. Above and below this region, however, measured values are considerably lower. The discrepancy cannot be analyzed readily but may be traced to the interference of the flow downstream of the grid by the tubes supporting the motor, equivalent to contravane effect, to secondary radial flow and to turbulent momentum transport, the latter resulting from instability of the outer boundary layer, for which no allowance has been made when accounting for skin friction, and finally at large quantities of discharge, that is, large values of w_m/u , to variations with radius of axial velocity component at outlet (see fig. 9) for which no correction has been made.

In consideration of this, the correlation is regarded as quite satisfactory.

CONCLUSIONS

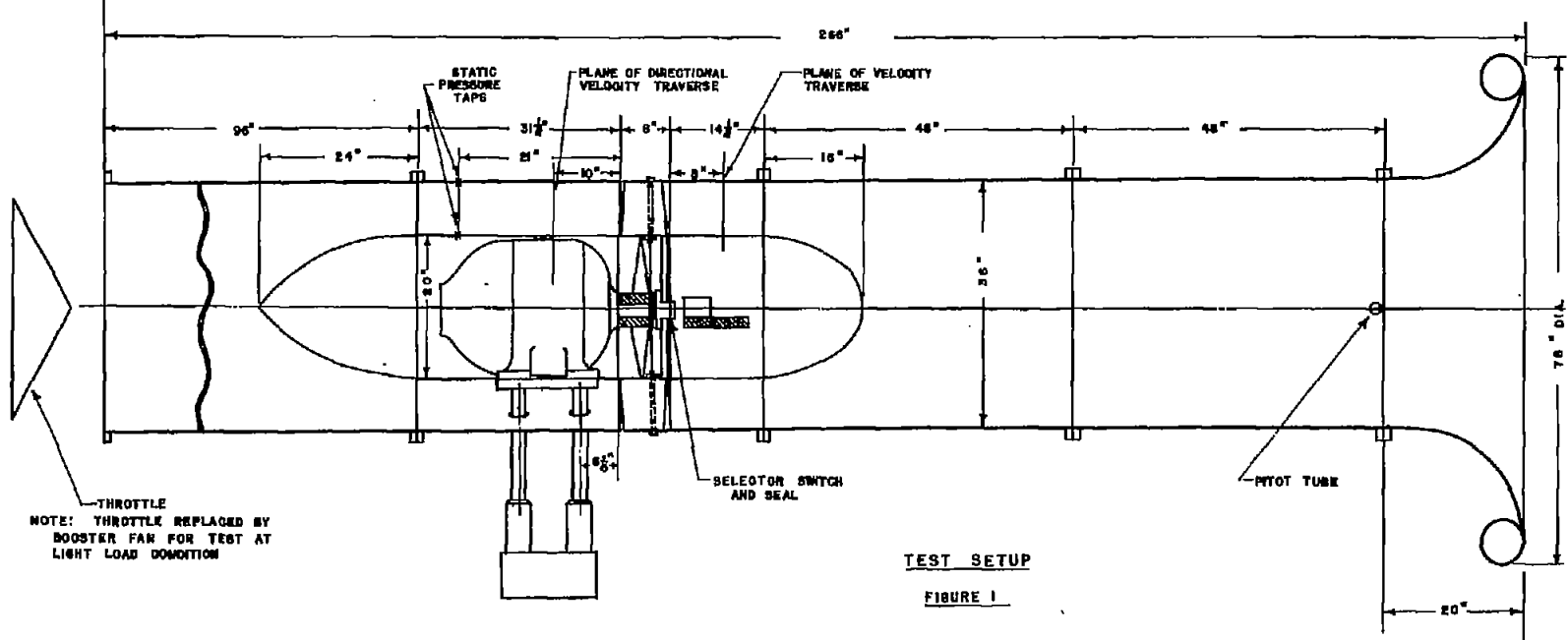
1. The profile lift characteristics, C_L versus α , for various stations of the rotating blade grid are linear over a range of angles of attack; their slope and corresponding aspect ratio varies from a maximum ($A = 6$) at midspan to very low values near the tip and root. These results suggest that the assumption of infinite aspect ratio made in the two-dimensional grid theory is inadequate for grids of the solidity and thickness ratio of the test grid.
2. The stalling points of the outer and the middle sections are closely interrelated; whereas the root section appears to maintain normal operation even after the flow past the outer section has separated, indicating that stalling spread from the outer section inward.
3. The inner station, that is, the profile near the root section, showed no tendency to stall at very high lift coefficients ($C_L = 1.4$) and at values of the circulation for which stall occurred at the tip and middle stations. It is concluded that rotating decelerating grids may be designed for lift coefficients at the root considerably above those accepted in present practice.
4. The polar curves of the various blade sections have a relatively narrow range of minimum drag coefficient (as a consequence of their low effective aspect ratio, conclusion 1, above). This renders their economical operating range quite critical. Furthermore, the maximum L/D ratio of the profile tested occurs at lift coefficients smaller than the design lift coefficient. Profiles of larger camber than that of the test section should be chosen for the root and midspan stations, for corresponding design operating conditions.
5. Radial displacement of the boundary layer and of the wake is a factor of major importance controlling the effective aspect ratio of the blade sections. Under certain conditions, such as those of the test grid, it causes separation of flow at the tip section before the root section approaches its stall point and thus precipitates "pumping" as a result of tip stall. Boundary layer removal at the tip is suggested as a means of restricting the pumping limit induced by tip stall.
6. Results of measurements of profile drag from oscillographs obtained with a hot wire placed stationary downstream of the rotating grid are in good agreement with those obtained by other means. The hot-wire method has the advantage of ready application and of simplicity and promises to give results of satisfactory accuracy, provided the hot

wire has the required directional and response characteristics.

Aerodynamics Laboratory,
Case School of Applied Sciences,
Cleveland, Ohio, May 1946.

REFERENCES

1. Weinig, Fritz: Die Strömung um die Schaufeln von Turbomaschinen.
J. A. Barth (Leipzig) 1935.
2. Ruden, P.: Investigation of Single Stage Axial Fans. NACA TM No. 1062, 1944.
3. Weske, John R.: Measurement of the Arithmetic Mean Velocity of a Pulsating Flow of High Velocity by the Hot-Wire Method. NACA TN No. 990, 1946.
4. Weske, John R.: Drag of Airfoils in Grids of High Solidity. Jour. Aero. Sci., vol. 11, no. 4, Oct. 1944, pp. 369-372.
5. Mutterperl, William: High-Altitude Cooling. VI - Axial-Flow Fans and Cooling Power. NACA ARR No. L411le, 1944.



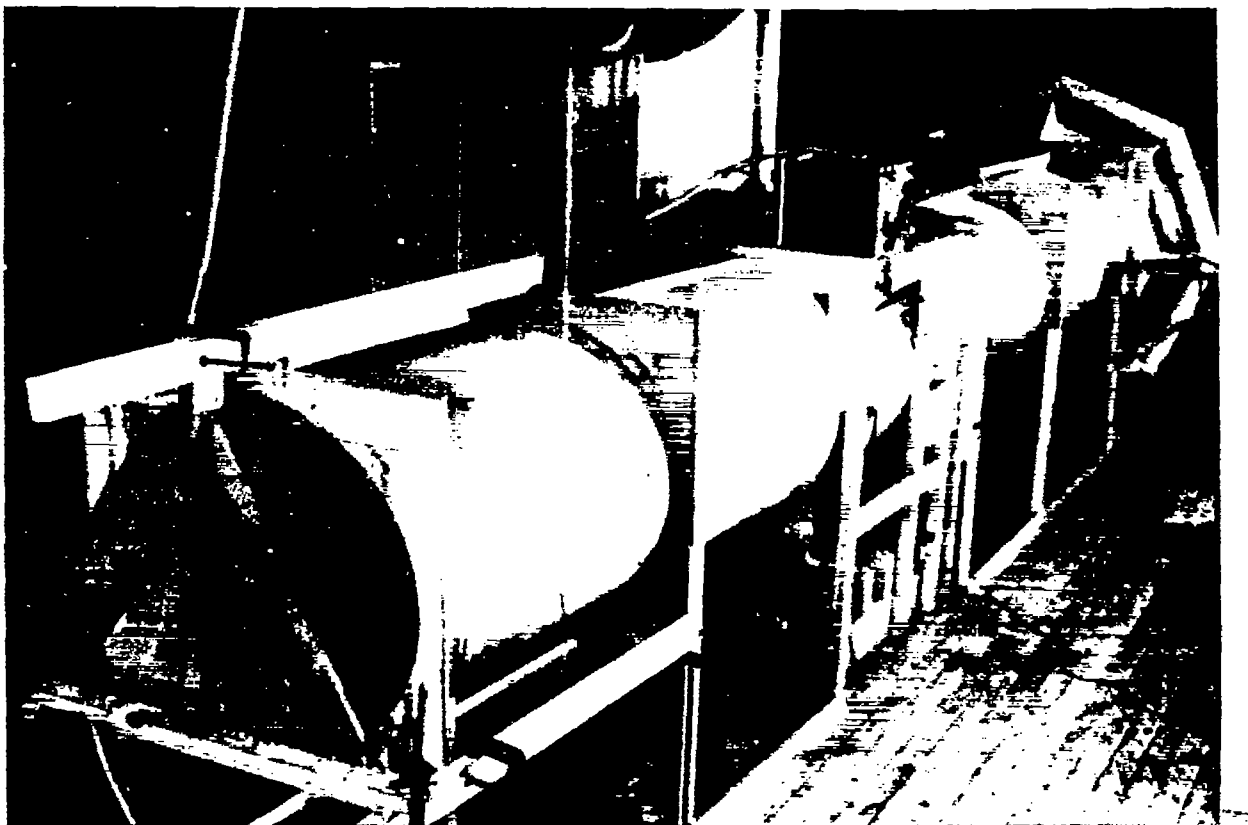


Figure 2.- Photograph of test setup from discharge side.

Fig. 3

NACA TN No. 1128

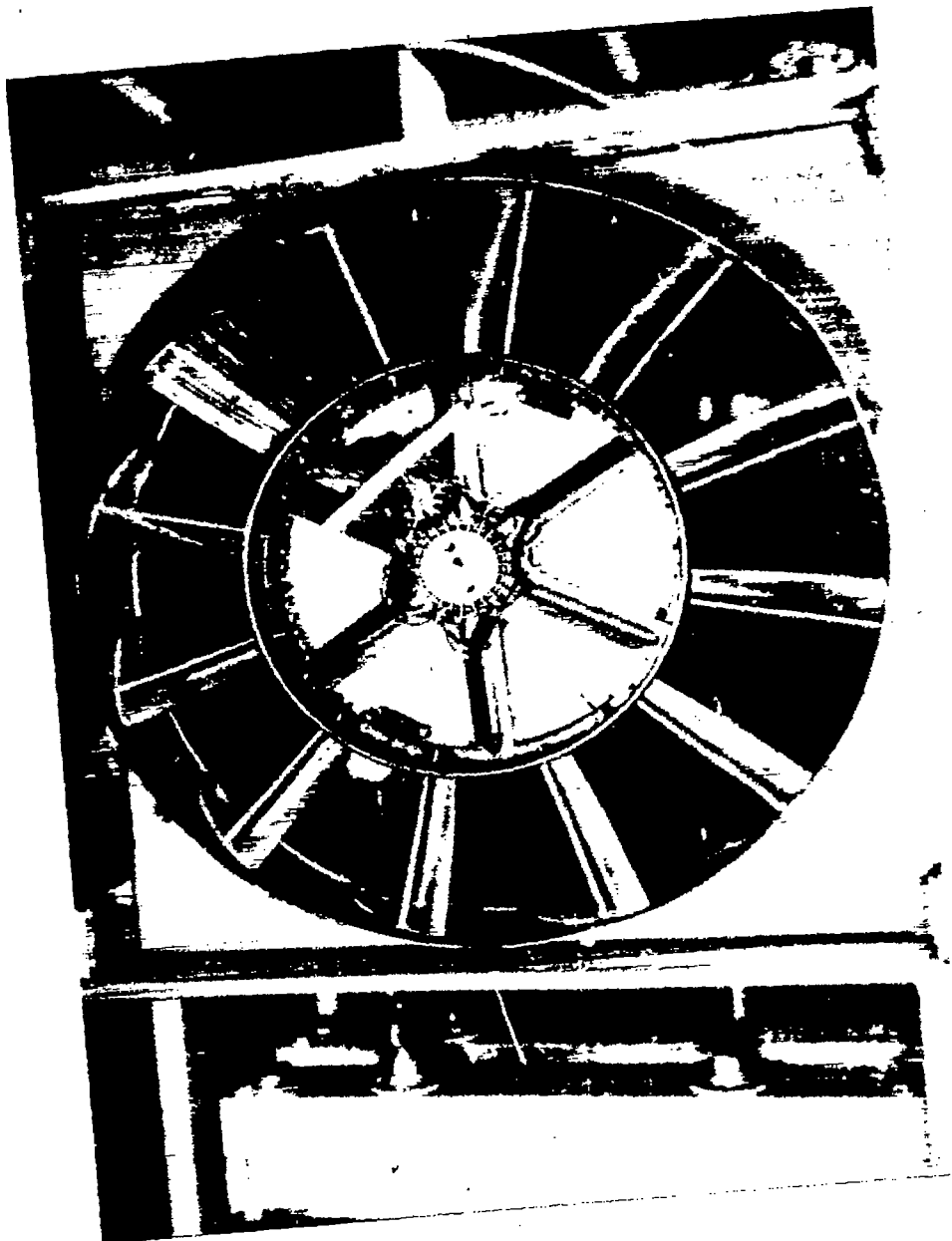


Figure 3.- View of the rotating grid showing the master blade, pressure leads, and rotating part of the selector switch.

Fig. 4

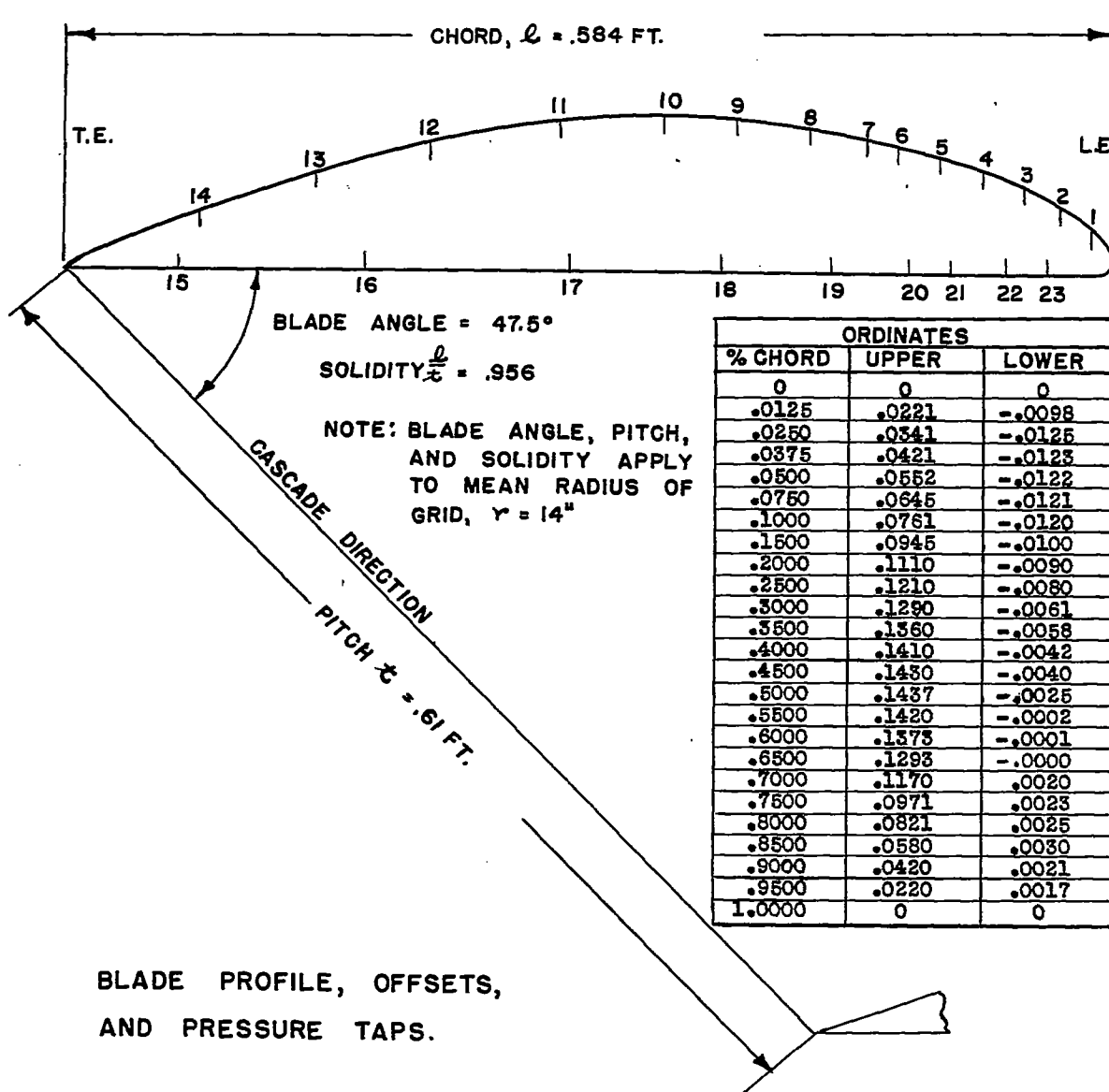


FIGURE 4.

NACA TN No. 1128

Fig. 5

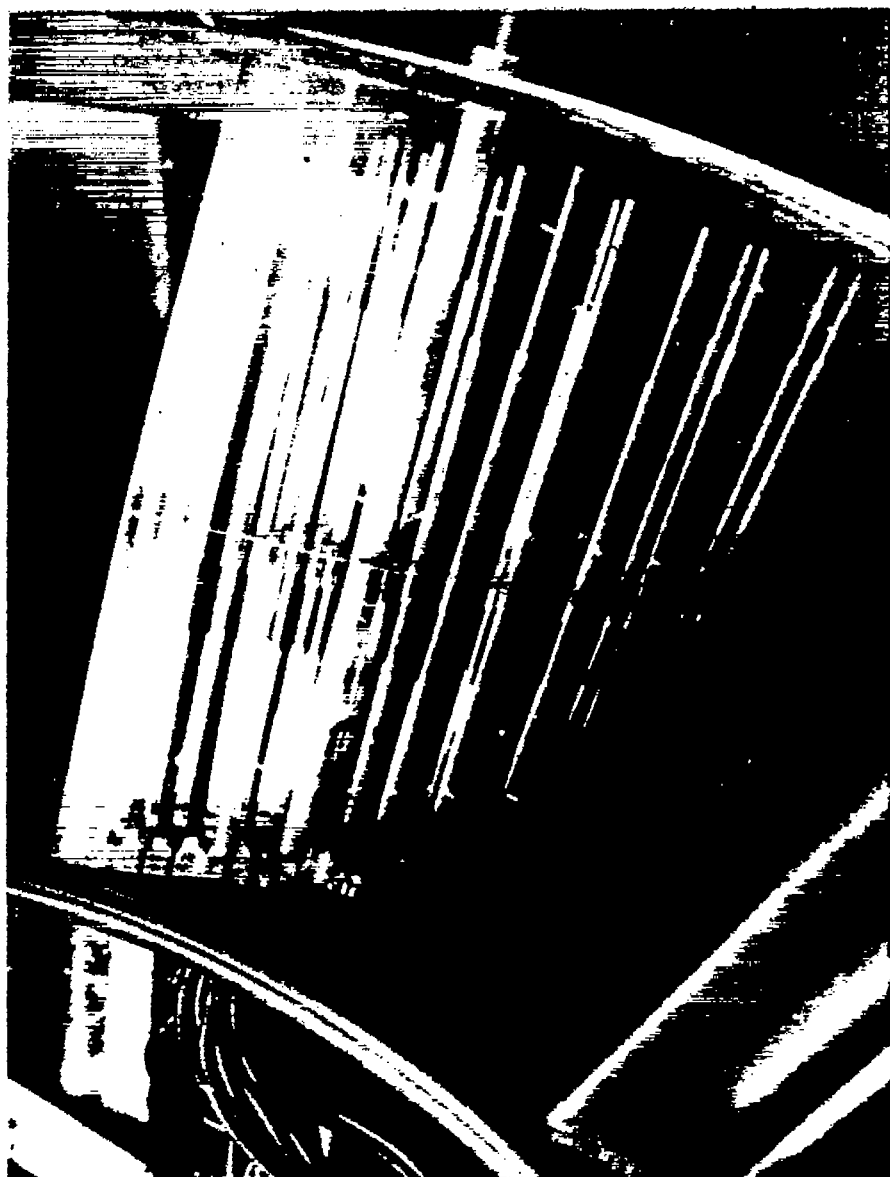


Figure 5.- Master blade.

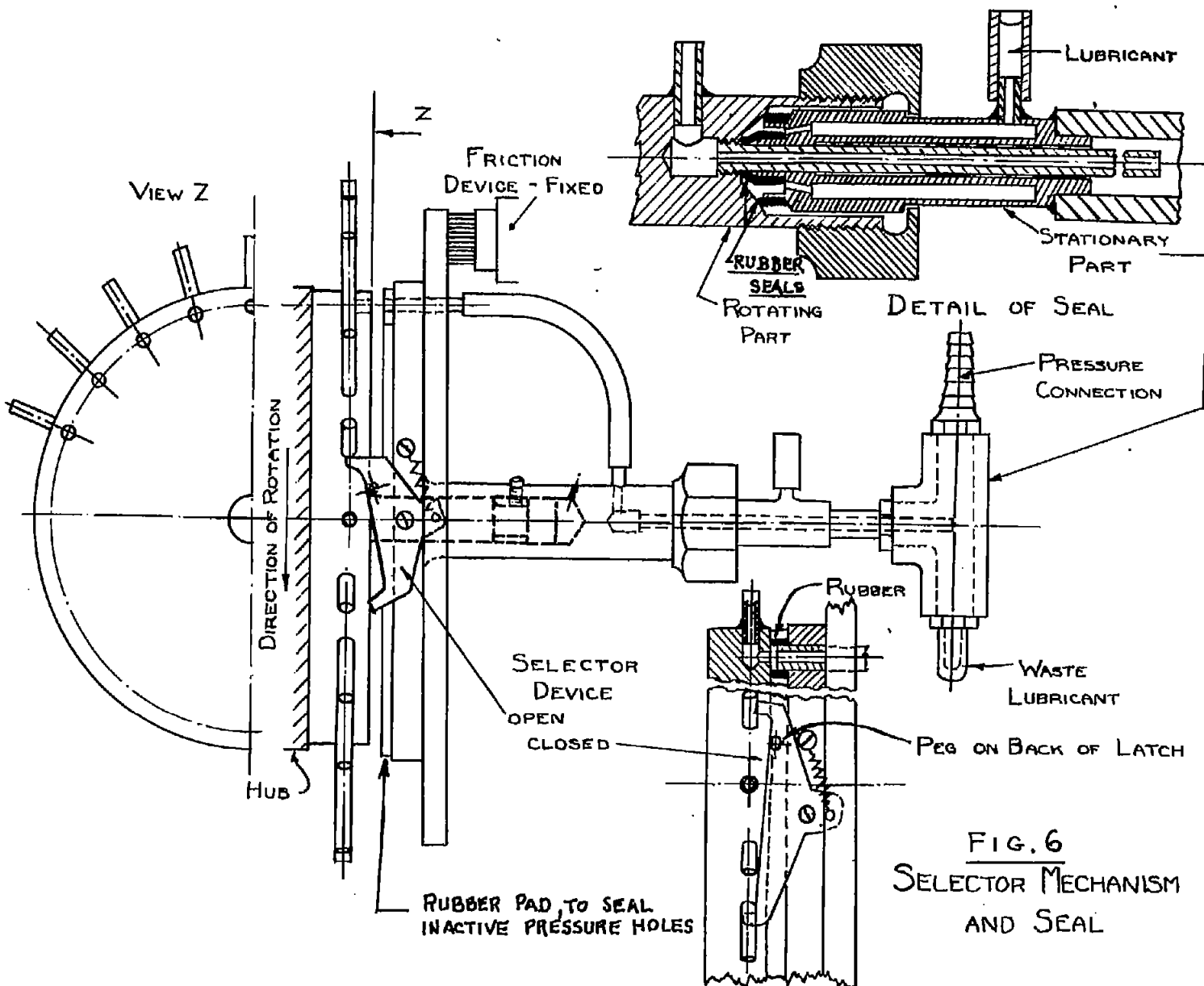
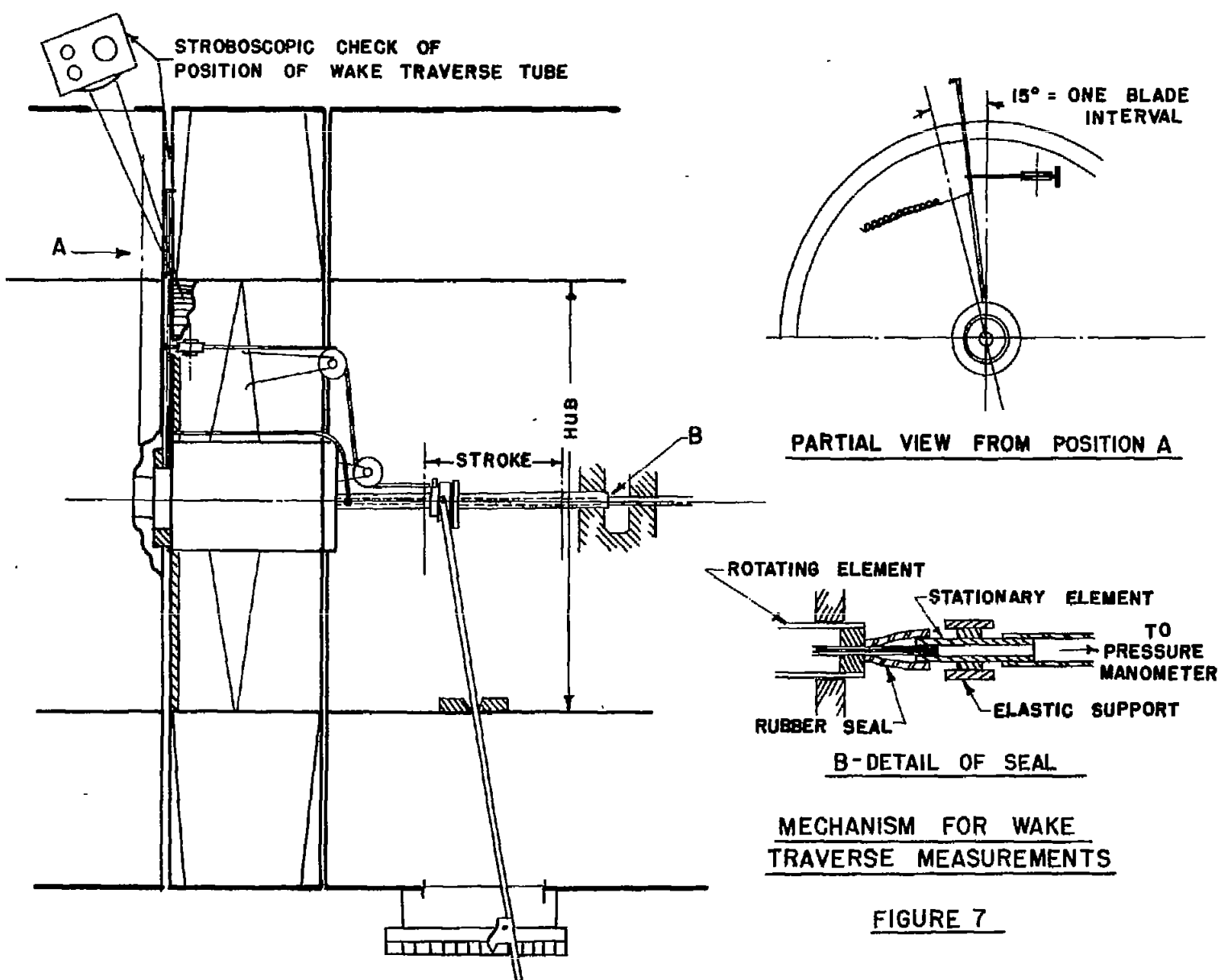
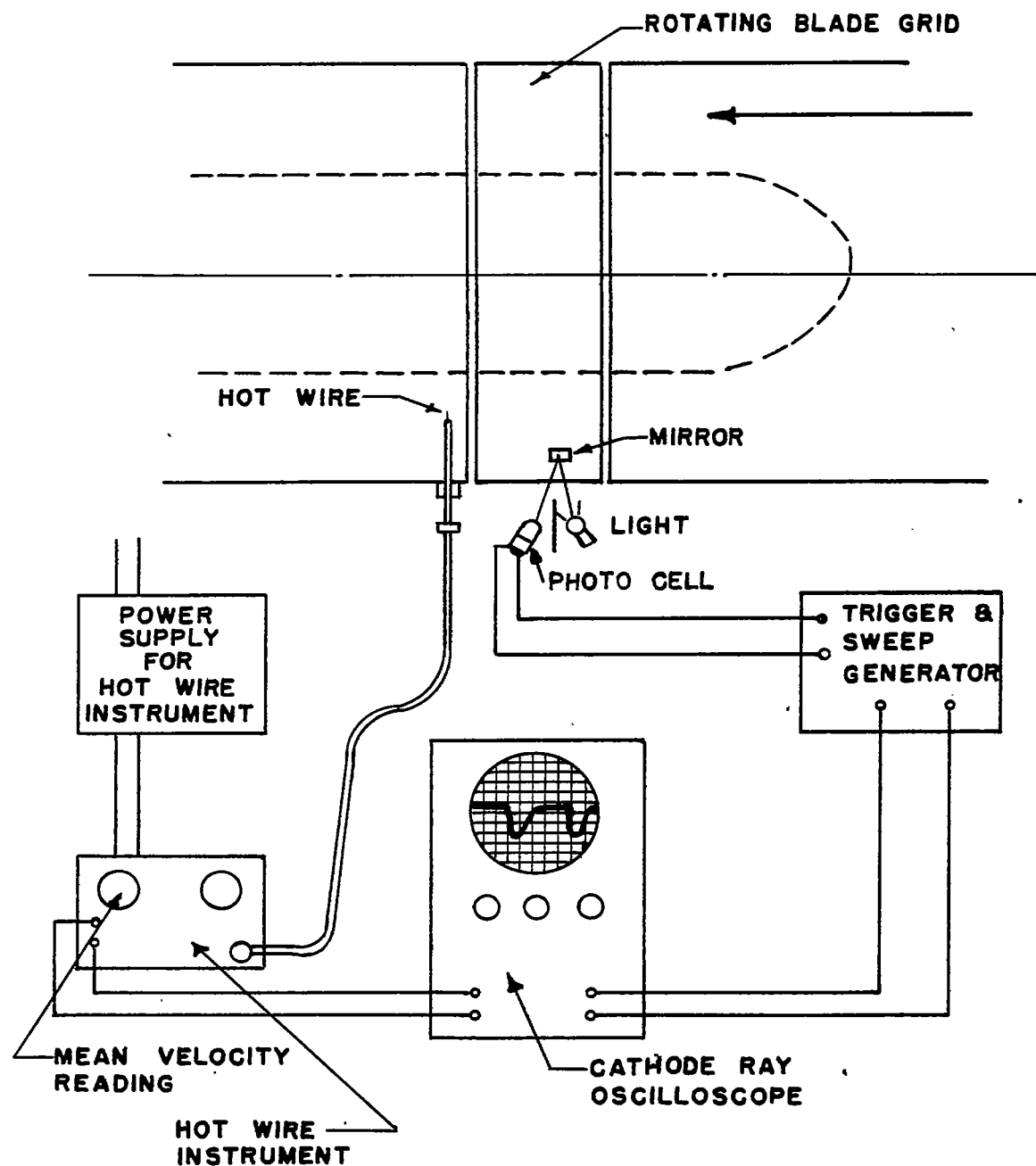


FIG. 6
SELECTOR MECHANISM
AND SEAL

Fig. 7

NACA TN No. 1128



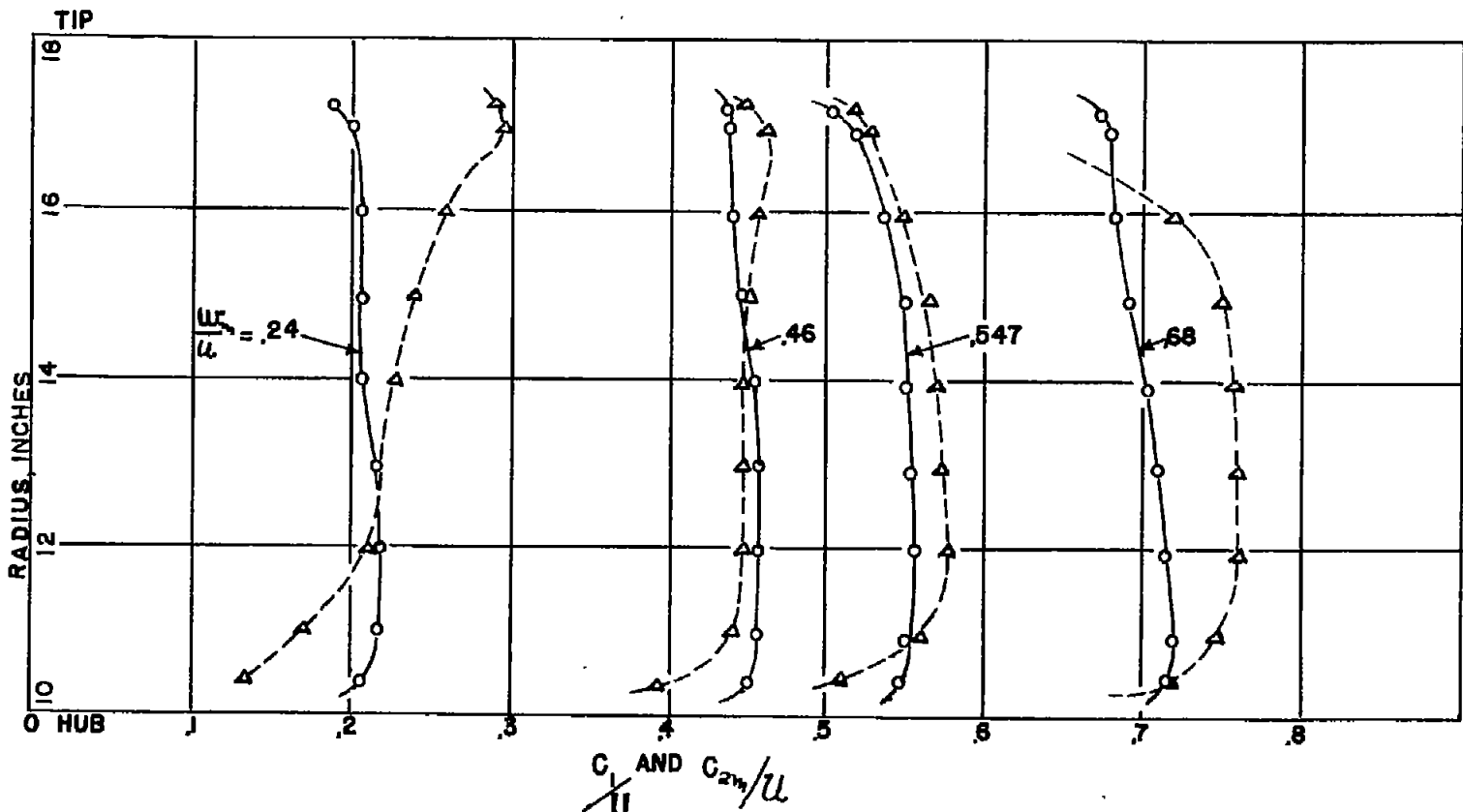


ARRANGEMENT OF HOT WIRE EQUIPMENT

FIGURE 8

Fig. 9

NACA TN No. 1128



PROFILE OF AXIAL VELOCITY
COMPONENT AT INLET AND
OUTLET OF GRID

—○— 8" UPSTREAM OF L.E. PLANE
---△--- 10" DOWNSTREAM OF T.E. PLANE

FIGURE 9.

Fig. 10a

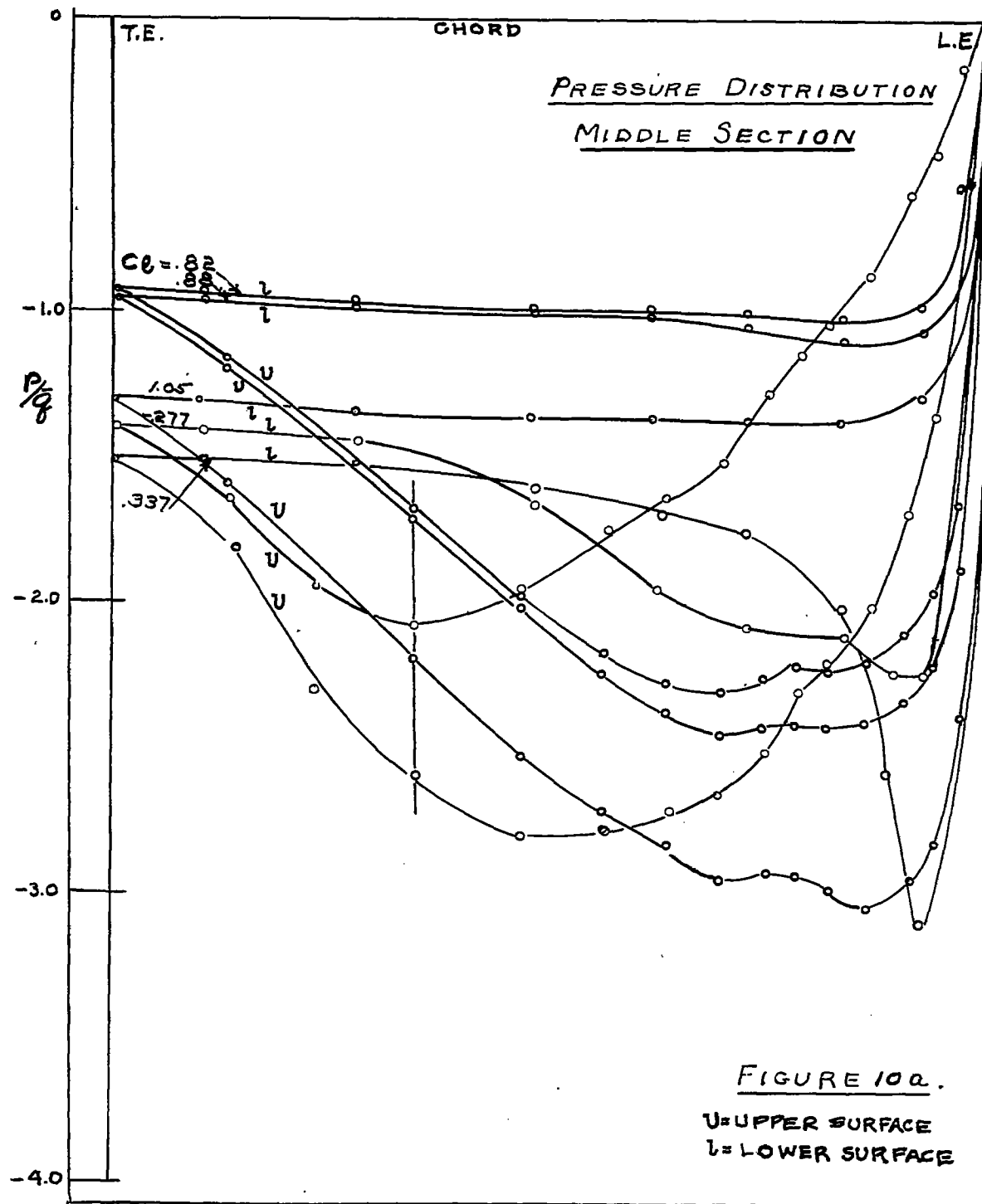


Fig. 10b

NACA TN No. 1128

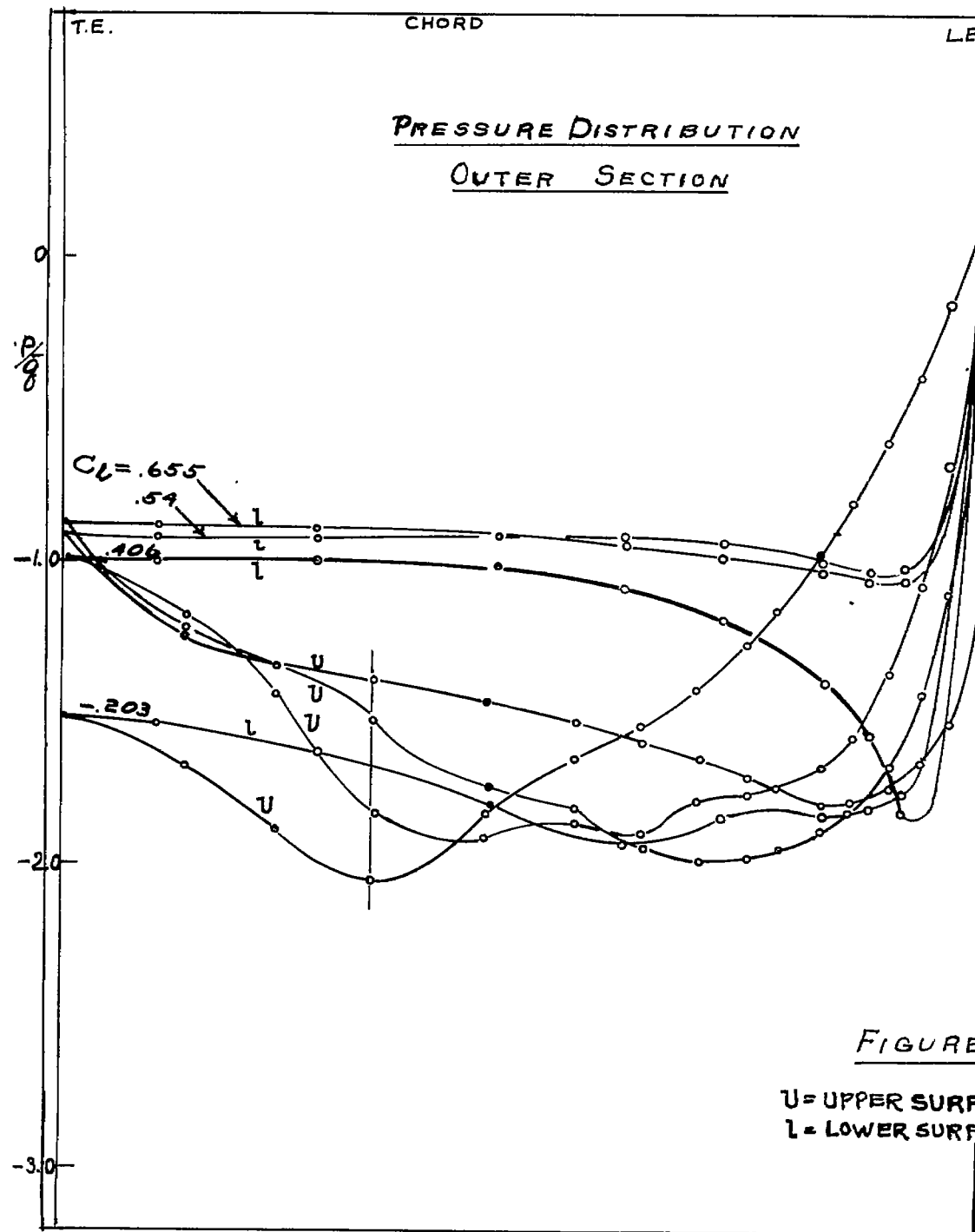


FIGURE 10,b

U = UPPER SURFACE
L = LOWER SURFACE

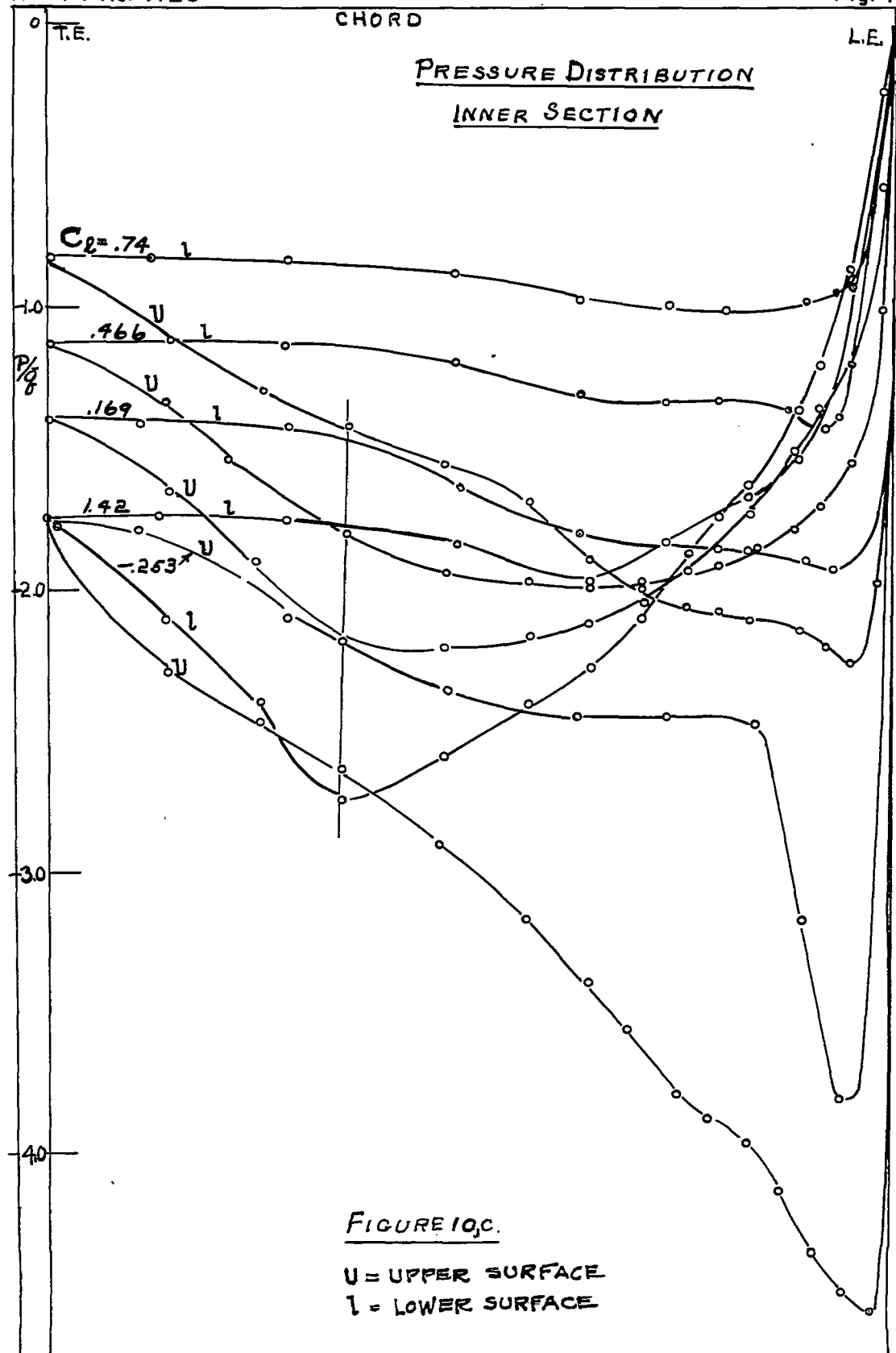


Fig. II

NACA TN No. 1128

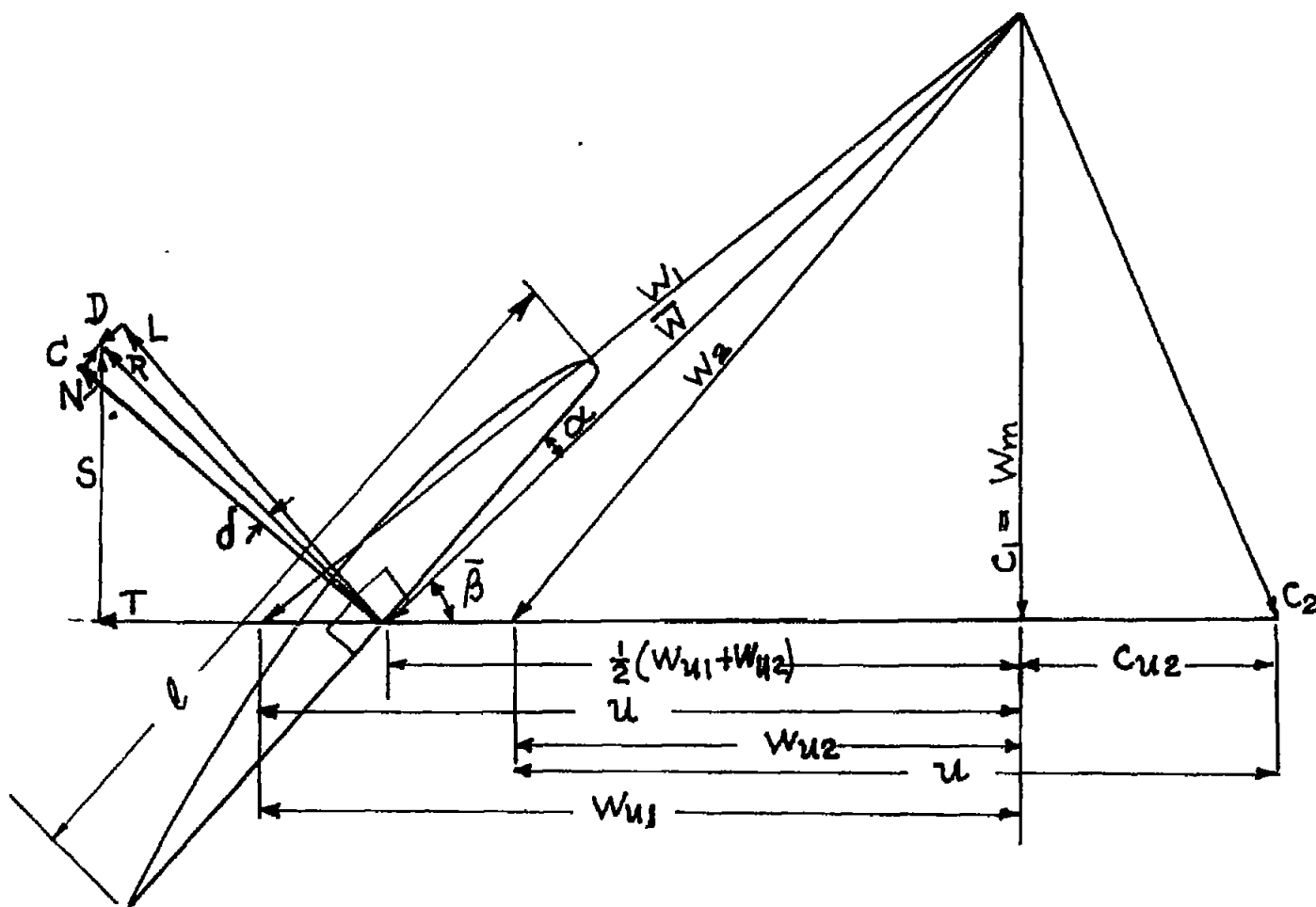


FIGURE II.
TYPICAL VELOCITY DIAGRAM
AND BLADE FORCES.

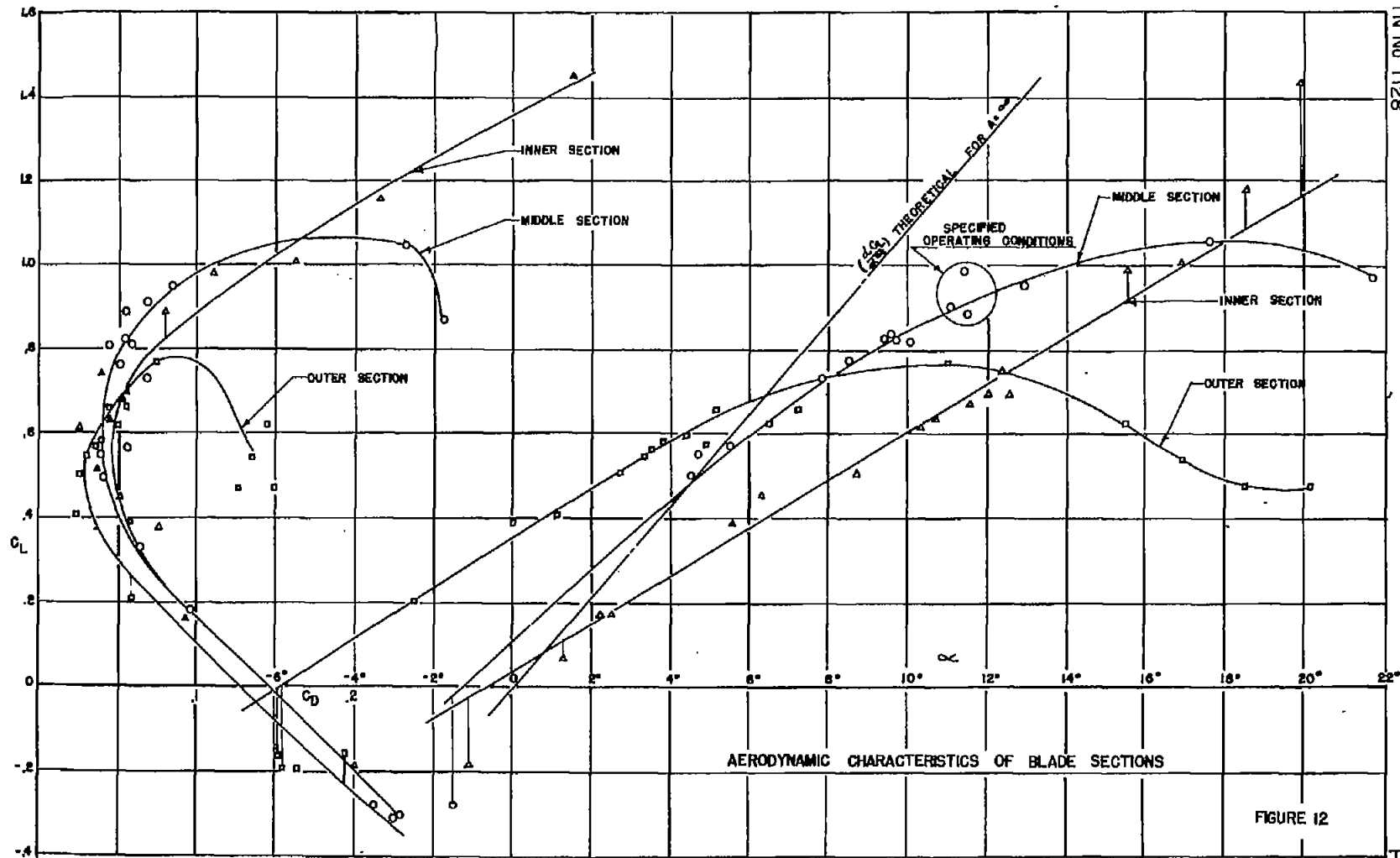
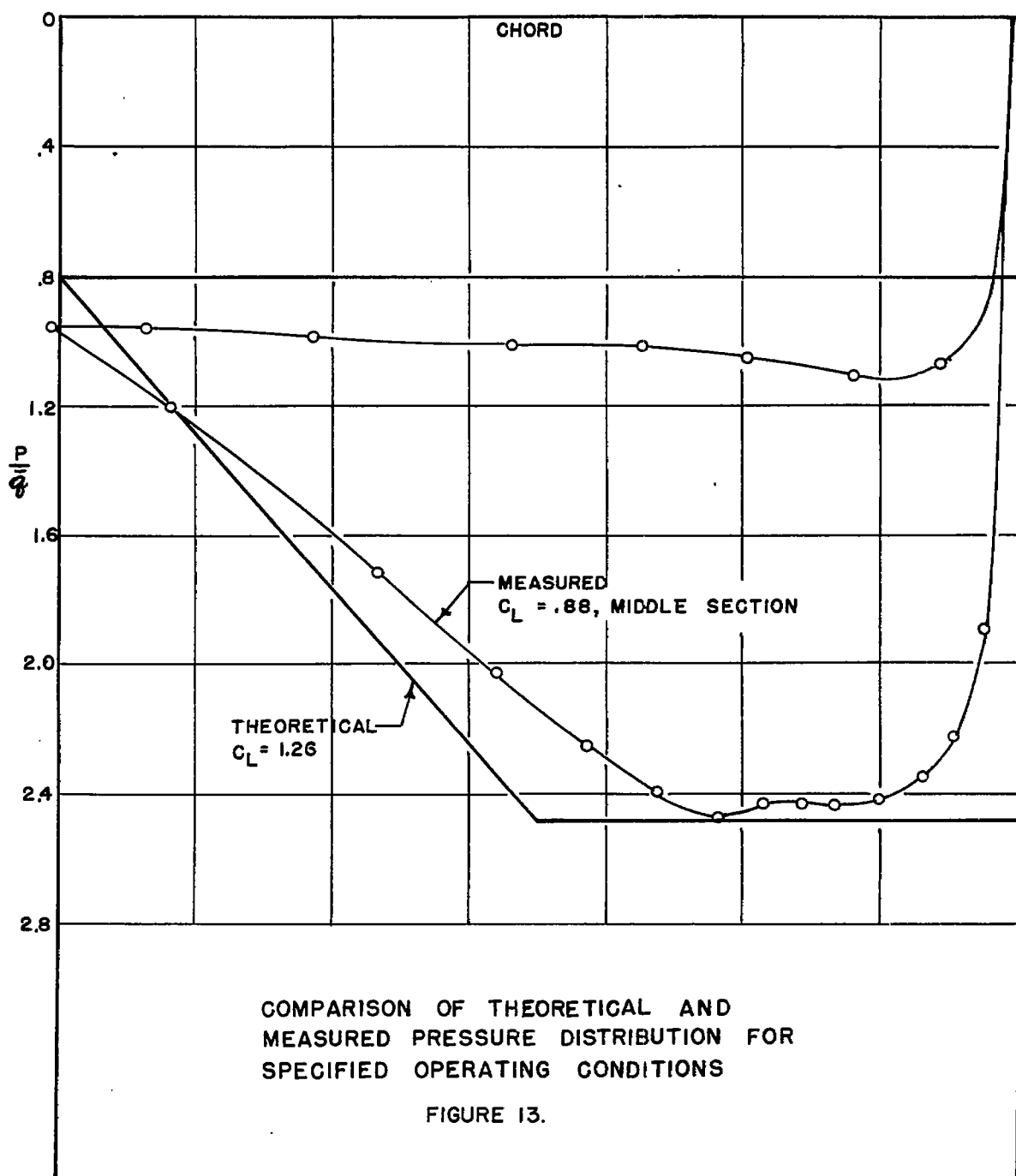


Fig. 13

NACA TN No. 1128



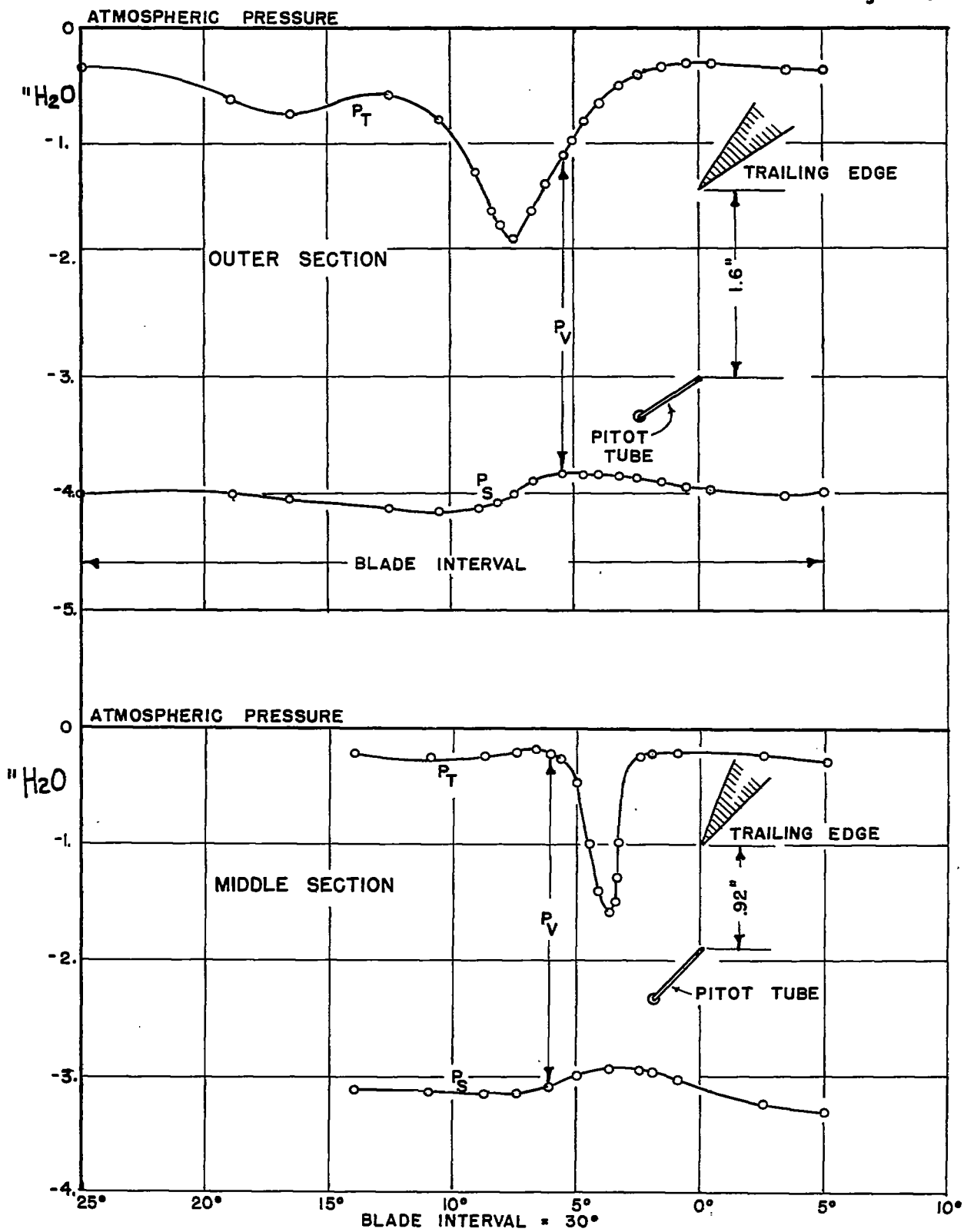


FIGURE 14a,b.— PITOT WAKE TRAVERSE MEASUREMENTS.

Fig. 14b

NACA TN No. 1128

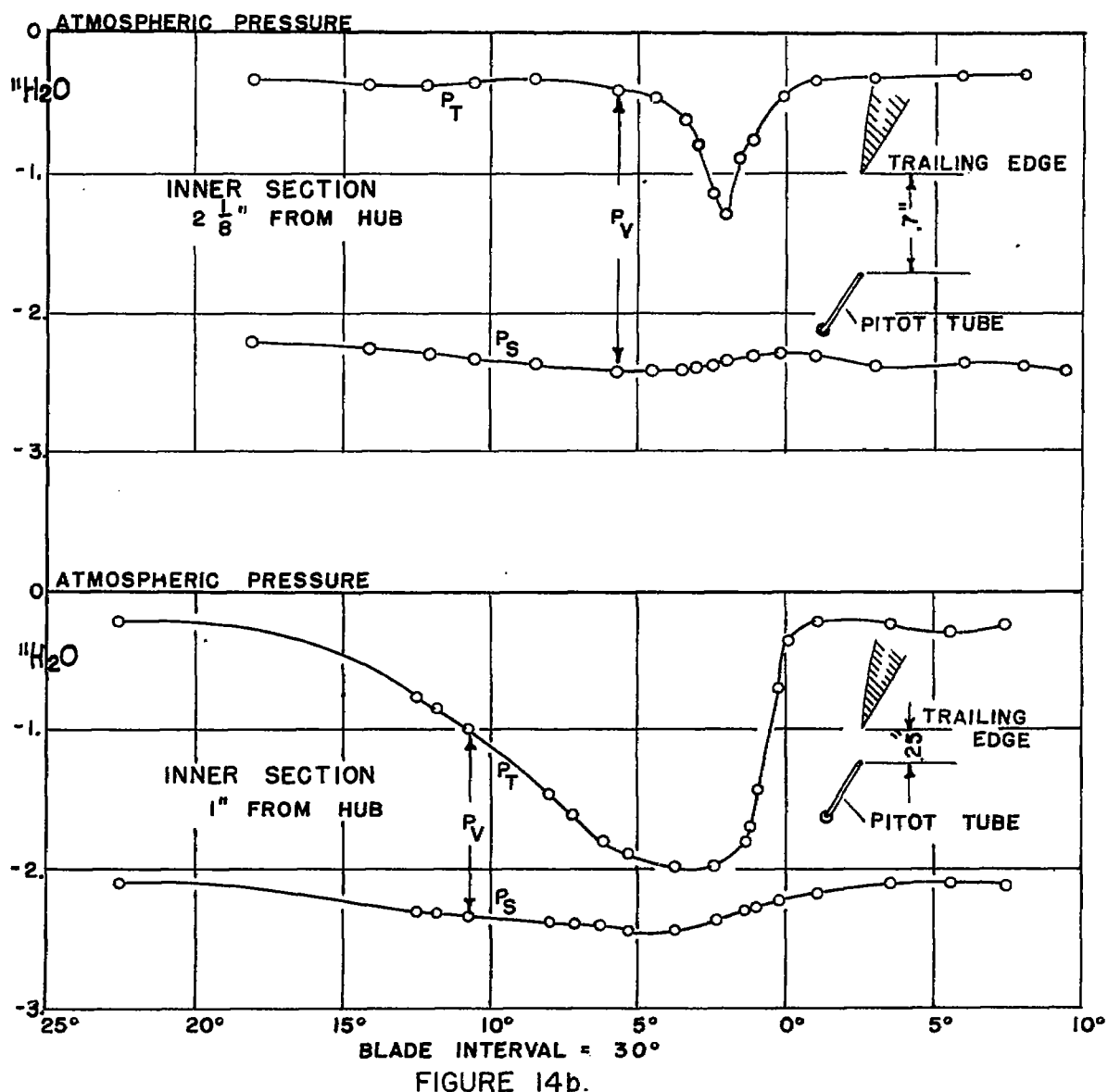




Figure 15.- Typical hot wire oscilloscope. Record of hot wire wake traverse of axial velocity components for middle blade station at lift coefficient of 0.72 and Reynolds number of 500,000.

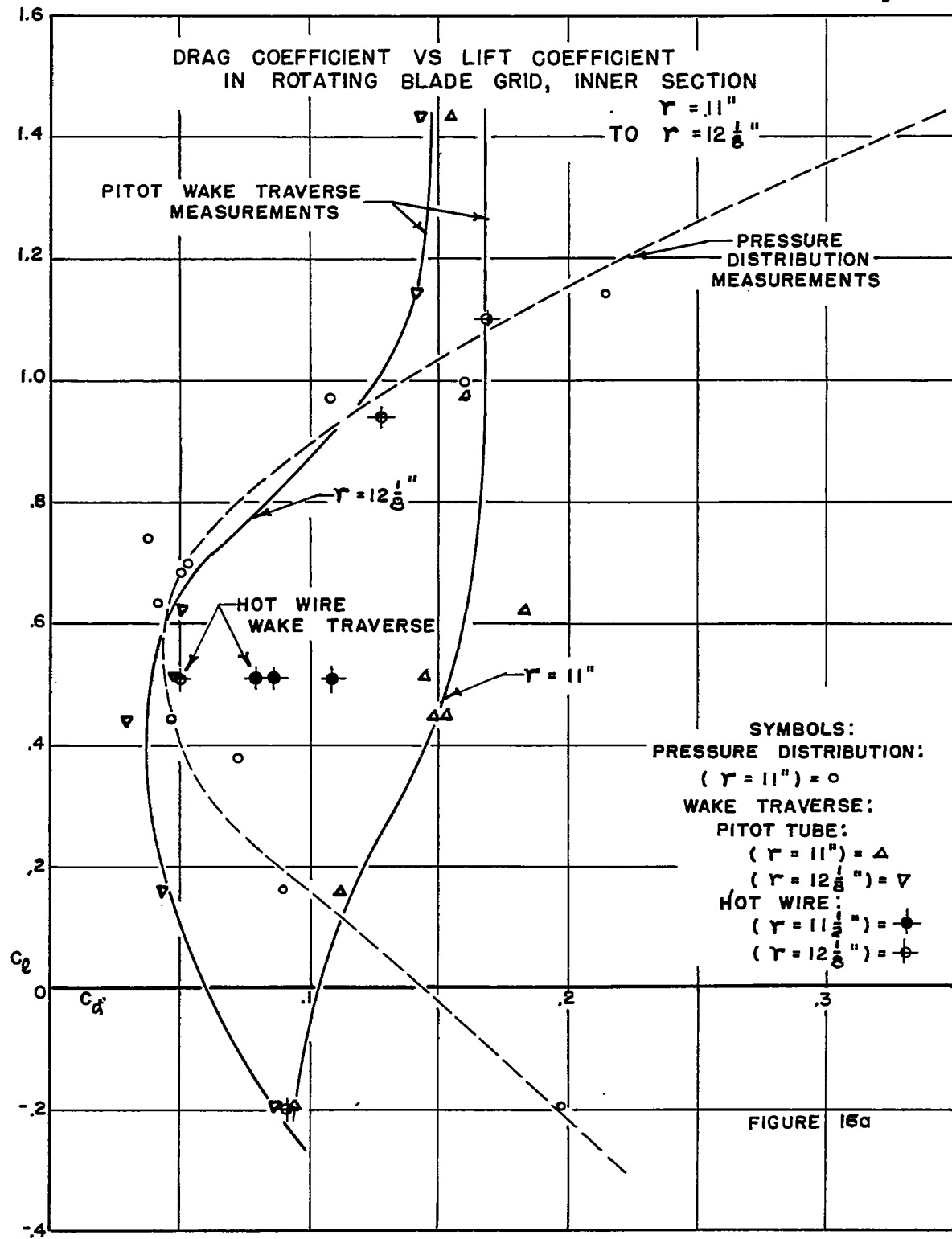
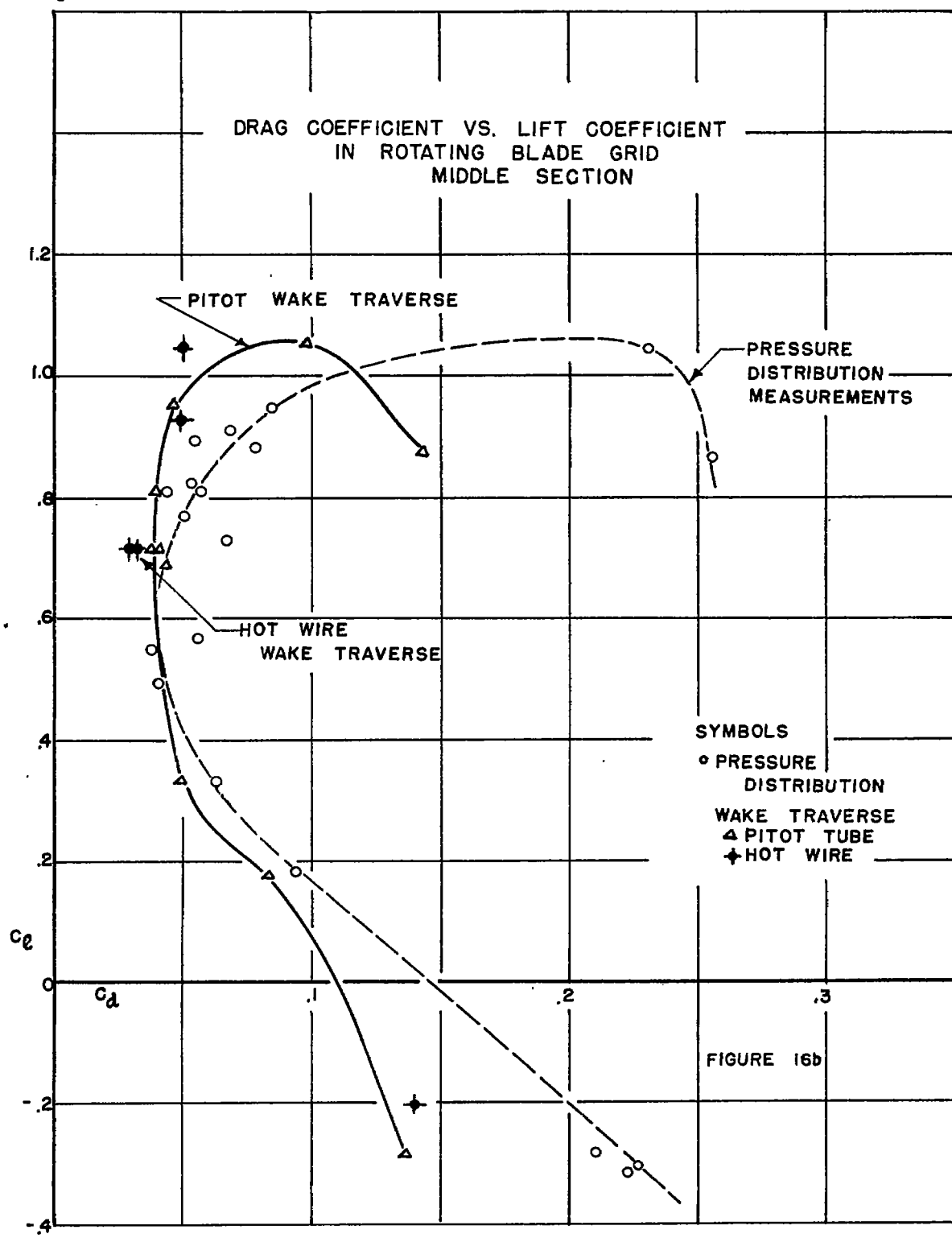


Fig. 16b

NACA TN No. 1128



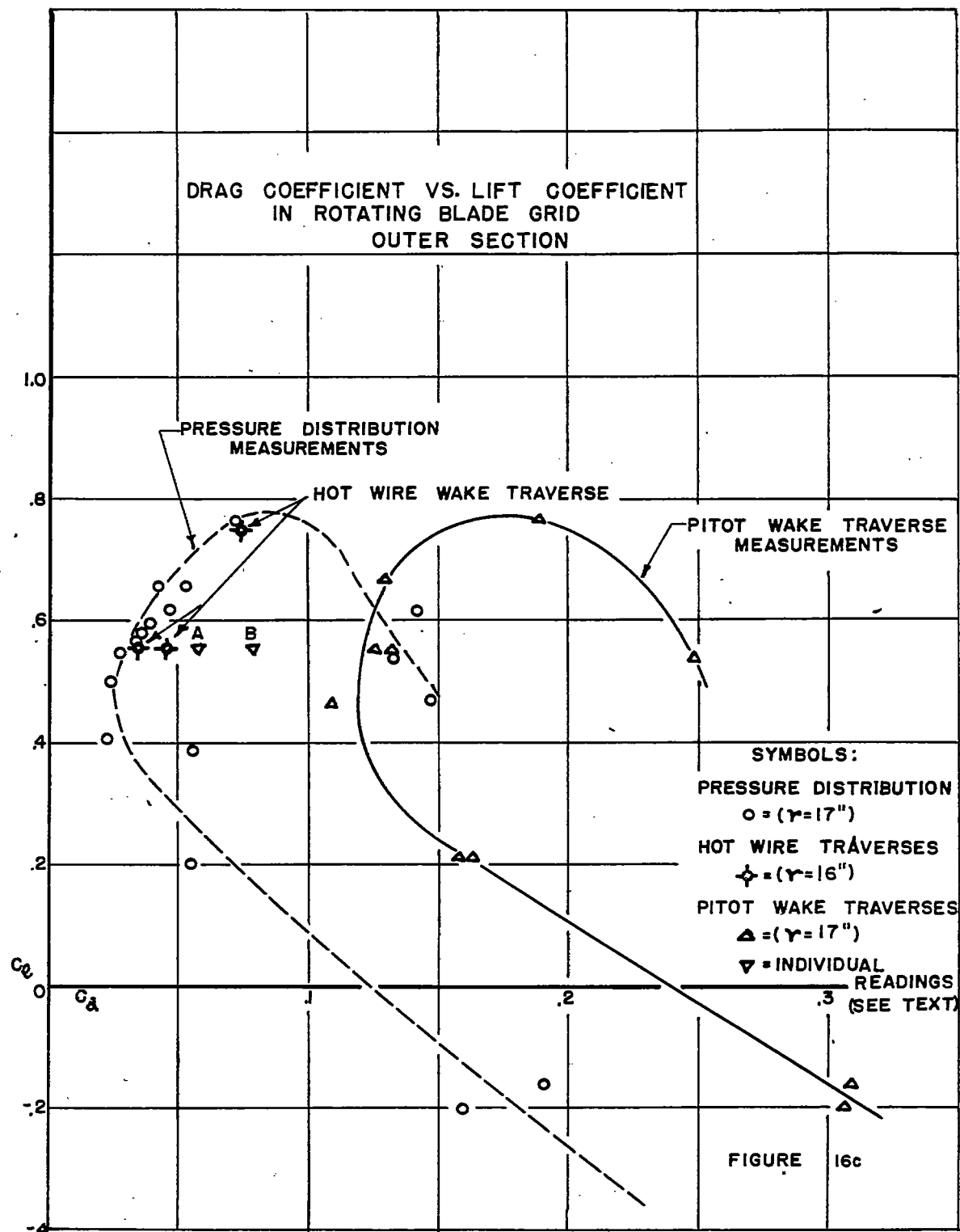
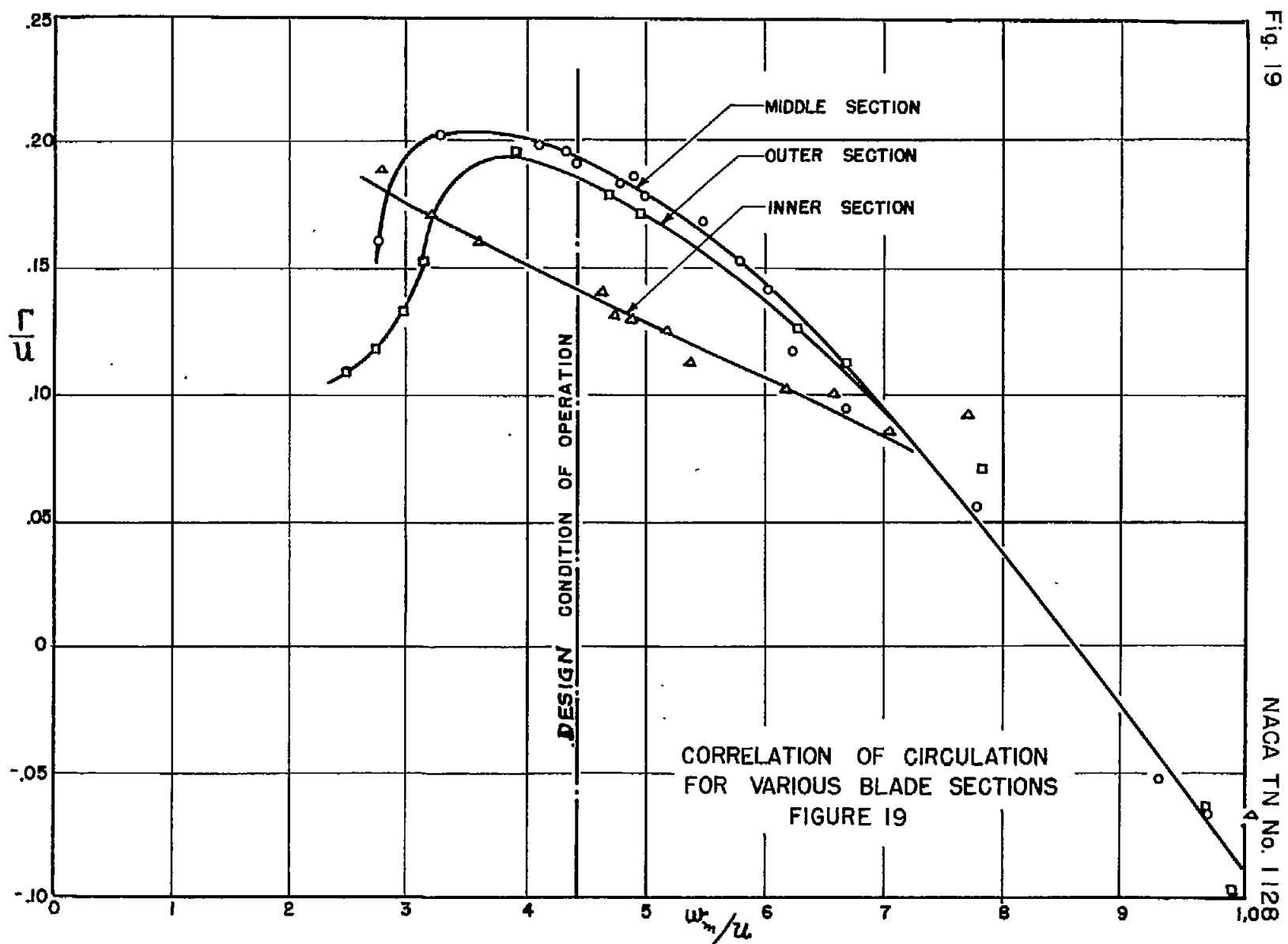


Fig. 19

NACA TN No. 1128



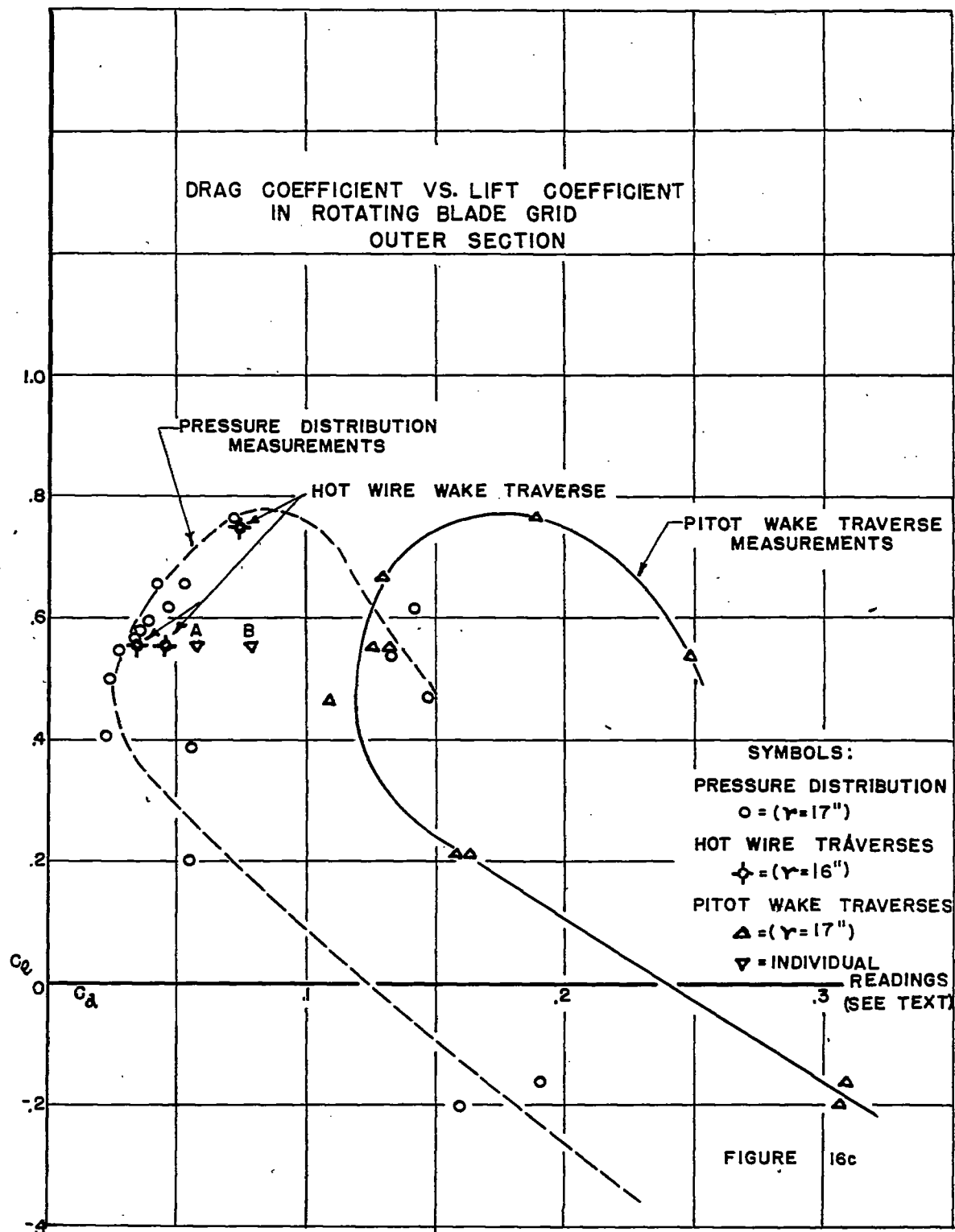


Fig. 17

NACA TN No. 1128

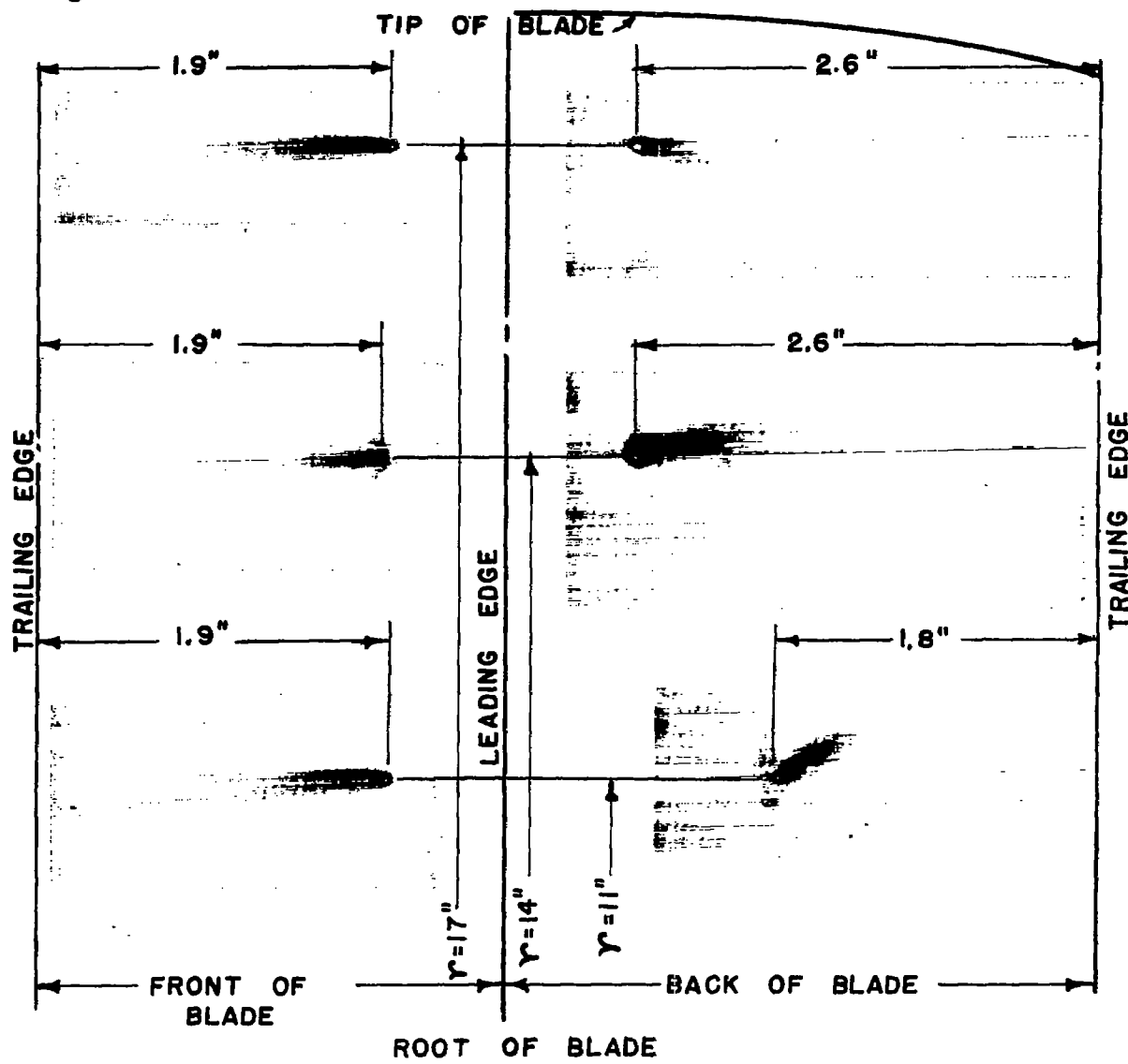


FIGURE 17.- DIRECTION OF FLOW IN THE BOUNDARY
LAYER OF THE MASTER BLADE IN THE
ROTATING GRID

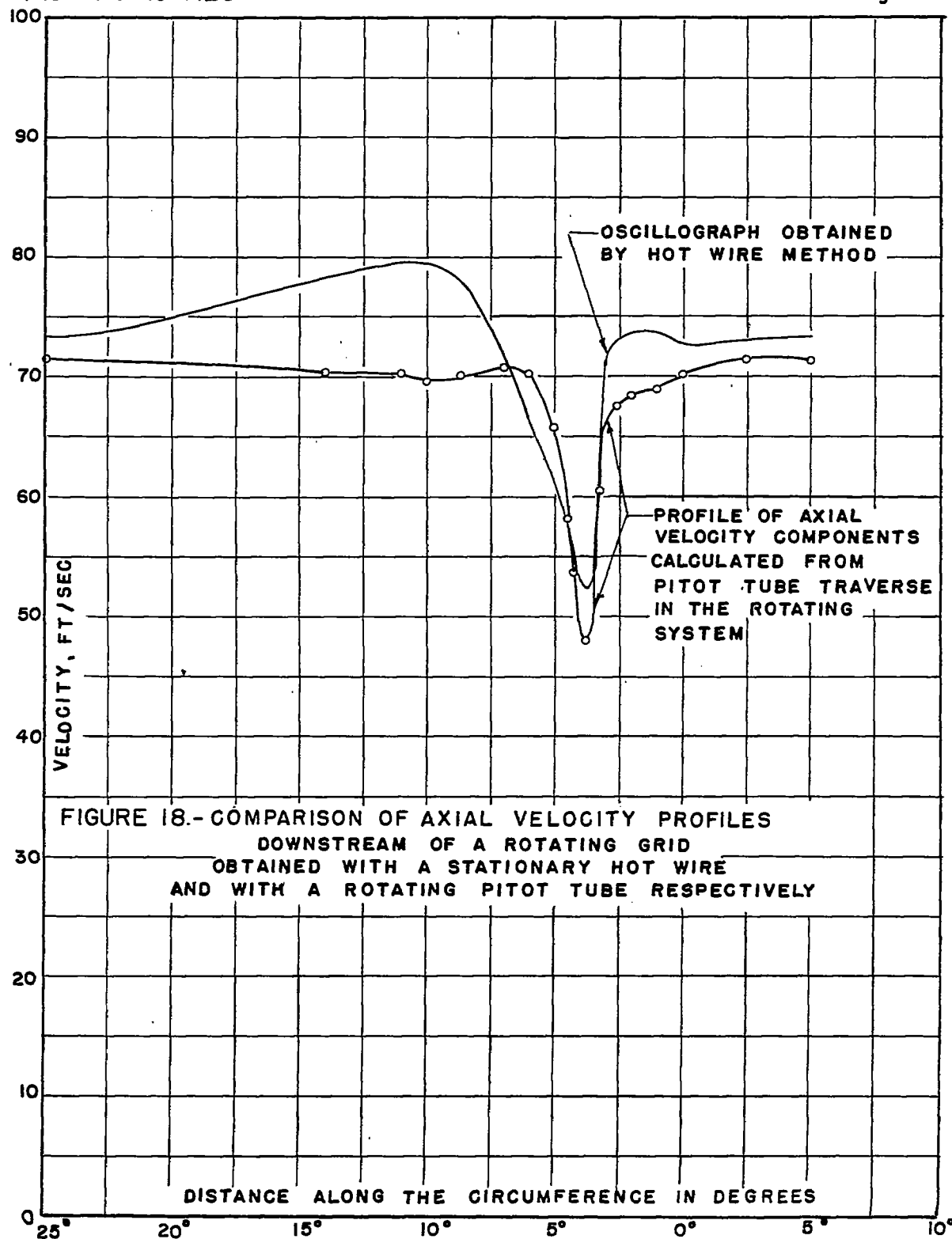


Fig. 19

NACA TN No. 1128

